International Communications in Heat and Mass Transfer 148 (2023) 107000

Contents lists available at ScienceDirect

International Communications in Heat and Mass Transfer

journal homepage: www.elsevier.com/locate/ichmt

Approximate semi-analytical technique based on eigenfunction expansion for phase change heat transfer in a cylindrical body contained within a thick multilayered annular wall

Emad Hasrati, Ankur Jain *

Mechanical and Aerospace Engineering Department, University of Texas at Arlington, Arlington, TX, USA

ARTICLE INFO

Keywords:
Phase change heat transfer
Melting
Solidification
Analytical modeling
Eigenfunction expansion
Multilayer cylinder

ABSTRACT

Phase change heat transfer occurs commonly in thermal management and energy storage problems. Most literature in this direction assumes direct contact between the phase change material (PCM) and the heat source/sink. However, in practical problems, the PCM is often enclosed within a non-melting wall. This work presents an approximate eigenfunction expansion-based analysis of inwards phase change propagation in a cylindrical PCM encapsulated in a multilayer annular wall. The model accounts for imperfect thermal contact between layers. The transient temperature distribution is determined by solving a transient multilayer thermal conduction problem. Evolution of the phase change front is determined by inserting the temperature distribution into the interfacial energy conservation equation. Results are shown to agree with past work for special cases of the general problem considered here. Good agreement with both experimental and numerical data from past work, and with finite-element numerical simulations is demonstrated. The role of key non-dimensional parameters on phase change characteristics, including total time to melt/freeze is quantified. Ranges of non-dimensional numbers in which the approximate method offers good accuracy are determined. This work extends the state-of-the-art of phase change modeling, with potential applications in energy storage, nuclear engineering, oil/gas transport, and in mass transport problems.

1. Introduction

Moving boundary problems involving solidification and melting occur commonly in science and engineering [1–4]. Common applications include thermal energy storage [5], thermal management [6] and manufacturing [7]. Additionally, problems involving mass transport and chemical reactions, such as combustion [8], silicon oxidation [9] and dissolution-limited drug delivery [10] also result in moving boundary problems. Improving the design and optimization of such devices and processes requires good theoretical understanding of the underlying heat/mass transfer moving boundary problem.

Due to their broad applications, moving boundary problems have been studied extensively. In addition to experimental measurements, an extensive body of theoretical methods has also been developed for predicting the evolution of the moving boundary [1,2] and total melting/solidification time [11] in such problems. One of the simplest moving boundary problem that appears in heat and mass transfer is that of one-dimensional melting/solidification of a Cartesian slab due to a high temperature imposed at one end of the slab. An exact solution for this problem presented by Stefan predicts a $\sqrt{t}$ dependence of the phase change front location [2,12]. The non-dimensional combination of heat capacity, latent heat and the imposed temperature (relative to the melting temperature), called the Stefan number, plays a key role in such problems [1–3].

Unfortunately, however, most realistic phase change problems present additional complications such as temperature-dependent properties [13], multi-dimensional phase change propagation [7], phase change over a temperature range [7], presence of non-melting materials [14,15] and space/time-dependent boundary conditions [16]. Such complications typically introduce additional non-linearities in the problem, making it difficult to derive an exact analytical solution. Nevertheless, due to the technological importance of such problems, a considerable amount of past literature has been devoted to the development of approximate methods and error estimation of such methods [1,2]. Amongst the most commonly used approximate methods to solve phase change moving boundary problems include quasi-steady methods [2], perturbation methods [16] and integral methods [17]. In addition, a

* Corresponding author at: 500 W First St, Rm 211, Arlington, TX 76019, USA.
E-mail address: jaina@uta.edu (A. Jain).

https://doi.org/10.1016/j.icheatmasstransfer.2023.107000

Nomenclature

C	heat capacity ($Jkg^{-1}K^{-1}$)
$\mathscr{L}$	latent heat of phase change (Jkg^{-1})
k	thermal conductivity ($Wm^{-1}K^{-1}$)
h	convective heat transfer coefficient ($Wm^{-2}K^{-1}$)
M	total number of layers
Z	thermal contact resistance, (Km^2W^{-1})
$\bar{Z}$	non-dimensional thermal contact resistance, $\bar{Z}_m = \frac{k_L Z_m}{R_0}$
Ste	Stefan number, $Ste = C_L(T_\infty - T_f)/\mathscr{L}$
Bi	Biot number, $Bi = hR_0/k_L$
T	temperature (K)
r	spatial coordinate (m)
a_{LS}	Phase change front location (m)
R_0	phase change material radius (m)
t	time (s)
α	thermal diffusivity (m^2s^{-1})
$\bar{\alpha}_m$	ratio of thermal diffusivities, $\bar{\alpha}_m = \frac{\alpha_m}{\alpha_L}$
$\bar{k}_m$	ratio of thermal conductivities, $\bar{k}_m = \frac{k_m}{k_L}$
τ	non-dimensional time, $\tau = \frac{\alpha_L t}{R_0^2}$
θ	non-dimensional temperature, $\theta_i = \frac{T_i - T_m}{T_{ref} - T_m}$, $i = L,1,2,\ldots,M$
ξ	non-dimensional spatial coordinate, $\xi = \frac{r}{R_0}$
χ_{LS}	non-dimensional phase change front location, $\chi_{LS} = \frac{a_{LS}}{R_0}$
λ	non-dimensional eigenvalue
γ	non-dimensional interface location, $\gamma_m = \frac{R_m}{R_0}$

Subscripts

f	phase change
in	initial temperature
L	liquid phase
LS	phase change front
m	layer number
∞	ambient

variety of numerical computation techniques have also been developed to solve complicated phase change problems. For example, reformulating the energy equation in terms of enthalpy instead of temperature is commonly used as the basis for numerical simulation of phase change problems [2]. Another common numerical technique involves taking a fixed spatial discretization of the phase change front and using the governing equations to determine the time taken for the phase change front to propagate to successive spatial locations [18].

The specific problem of phase change propagation in a cylinder has been investigated extensively, with applications in nuclear fuel rods [19], sub-sea transport of oil/gas [20], packed bed thermal energy storage [21] and pipeline glaciation in salt water [22]. Both inward and outward melting/solidification in a cylinder has been analyzed through analytical [23–25] and numerical [11,22,26–28] methods. In such papers, the cylindrical phase change material is usually assumed to be directly heated/cooled by an external medium, and the presence of any containing walls around the PCM is explicitly ignored. Such an assumption is likely reasonable when the solid wall around the PCM is thin and/or of sufficiently large thermal diffusivity. However, there may be several scenarios where this may not be an accurate assumption. For example, the wall is often needed to be reasonably thick in order to provide mechanical strength. Moreover, a low thermal conductivity material may often be preferred for cost and other considerations. Further, the wall may often be multilayer in nature due to structural and other reasons.

In scenarios such as those listed above, it is inaccurate to ignore the presence of the non-melting wall around the cylindrical PCM. While an exact analytical solution is unlikely in this case, nevertheless, an approximate analytical solution is still of much value for design and optimization. While eigenfunction expansion-based methods have been used in the recent past to analyze phase change in the presence of a multi-layer Cartesian wall [14], or an encapsulated spherical PCM [15], such results are not readily applicable to a multilayer cylindrical geometry. Such past work on Cartesian and spherical geometries is based on assuming the temperature distribution at any time to be the solution of a transient thermal conduction problem that satisfies the various boundary and interface conditions, which is then substituted into the energy conservation equation at the interface to determine the phase change front location. Utilizing this technique to solve the multilayer cylindrical phase change problem is of much interest and relevance to a variety of engineering problems, such as those summarized above. The use of this transient technique for solving cylindrical phase change problems has been presented before [29], but this work did not account for a finite-thickness wall around the PCM.

This work presents an approximate eigenfunction expansion-based theoretical analysis of phase change propagation in a cylindrical phase change material surrounded by multiple annular layers of non-melting materials. The general analysis presented here accounts for an arbitrary number of layers, as well as thermal contact resistance between layers. Good agreement of the present model with experimental data and numerical computation for special cases reported in the past is demonstrated. The theoretical results are used to analyze the impact of key non-dimensional parameters on phase change propagation. While the method used here is inherently approximate, the ranges of non-dimensional parameters is which good accuracy may be expected are determined. Results presented here are expected to aid in the design and optimization of a number of engineering devices and systems containing a cylindrical PCM surrounded by a thick homogeneous or multilayered wall.

2. Problem definition

Consider a long, axisymmetric cylindrical phase change material with radius R_0, surrounded by an M-layered encapsulation as illustrated in Fig. 1(a). As shown in Fig. 1(b), the m^{th} layer extends between $r = R_{m-1}$ and $r = R_m$, and has a thickness of $\delta_m = R_m - R_{m-1}$ for $m = 1,2,\ldots, M$. The outer surface of the composite structure is exposed to convective heat transfer with coefficient h to an ambient fluid of temperature T_∞. The problem of melting of a solid is considered here, although the technique and results are equally valid for the opposite problem of solidification. The entire cylindrical PCM is assumed to be initially solid at its melting temperature T_f ($T_f < T_\infty$). For generality, the initial temperature of each layer of the encapsulant is taken to be $T_{m,in}$ ($m = 1,2,\ldots, M$). As time passes, heat first conducts through the various encapsulant layers, and then diffuses into the PCM to cause melting. The position of the melting front, referred to as $a_{LS}(t)$, is a function of time. $a_{LS}(t)$ is measured radially inwards from the outer boundary of the PCM ($r = R_0$), and, therefore, $a_{LS}(t)$ is zero initially and attains a value of R_0 when the PCM is fully melted. Thermal conductivities and thermal diffusivities of the encapsulant layers are denoted by k_m and α_m, respectively. Similar properties for the liquid phase of the PCM are denoted by k_L and α_L, respectively. Since the solid is assumed to be initially at the melting temperature, therefore, no heat transfer into the solid phase occurs, and, therefore, thermal properties of only the liquid phase are important. A thermal contact resistance Z_m is assumed between the adjacent m^{th} and $(m\text{-}1)^{th}$ encapsulant layers ($m = 1,2,\ldots,M-1$), as shown in Fig. 1. In addition, the thermal contact resistance between the PCM and the first layer of the encapsulant is denoted by Z_L. This resistance may be of

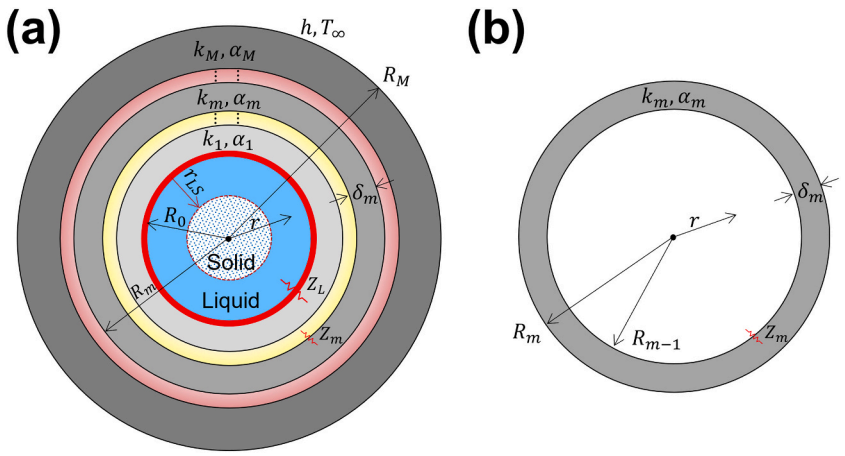

Fig. 1. Schematic geometry of the problem: (a) A one-dimensional cylindrical PCM encapsulated by a M-layer non-phase change wall, subjected to convection from a high temperature on the outer surface with a thermal contact resistance between layers; (b) details of the m^{th} layer.

particular relevance for the solidification problem, in which the innermost layer of the cylinder contacts the recently solidified phase change material. The general interest here is to determine the temperature distribution in the melted PCM and encapsulant layers, as well as the location of the phase change as a function of time. Additionally, the total time taken for complete melting is a key performance parameter that is often of practical importance.

Several simplifications may be made in order to analyze the problem defined above.

1. Based on a long and axisymmetric geometry, a one-dimensional radial temperature distribution is assumed.
2. Several heat transfer mechanisms such as natural convection and radiation are neglected, which is usually justifiable when the temperature differences in the problem are relatively small.
3. All thermal properties are assumed to be uniform and independent of temperature.
4. The phase change process is assumed to occur at a fixed sharp phase change temperature, and not over a temperature range. Therefore, there is no two-phase mushy zone at the solid-liquid interface.

Note that the phase change front in this problem moves inwards with time, which makes this moving boundary problem more complicated than a problem with fixed boundaries. As an approximation, the temperature distribution at any instant in time is determined by solving the transient thermal conduction problem up to that point. Based on the assumptions discussed above, the governing energy conservation equations for the transient temperature distributions in the encapsulant and PCM may be written as follows

$$\frac{1}{r}\frac{\partial}{\partial r}\left(r\frac{\partial T_m}{\partial r}\right)=\frac{1}{\alpha_m}\frac{\partial T_m}{\partial t}, \qquad (R_{m-1}<r<R_m, m=1,2,\ldots,M) \tag{1}$$

$$\frac{1}{r}\frac{\partial}{\partial r}\left(r\frac{\partial T_L}{\partial r}\right)=\frac{1}{\alpha_L}\frac{\partial T_L}{\partial t}, \qquad (R_0-a_{LS}(t)<r<R_0) \tag{2}$$

where $T_m(r,t)$ and $T_L(r,t)$ represent the temperature fields in the m^{th} encapsulant layer and the liquid phase of the PCM, respectively. Based on the assumption of the PCM being initially at the melting temperature, there is no heat transfer into the solid phase, and, therefore, there is no need to compute the solid temperature field. This approximation that distinguishes between Stefan and Neumann problems is often made in the modeling of phase change problems [2–4].

Convective heat transfer at the outer boundary may be written mathematically as

$$-k_M\frac{\partial T_M}{\partial r}=h(T_M-T_\infty), \qquad (r=R_M) \tag{3}$$

At the phase change front located at the other end of the geometry, the liquid must be at the melting temperature, i.e.,

$$T_L=T_f, \qquad (r=R_0-a_{LS}(t)) \tag{4}$$

Further, energy conservation and thermal contact resistance at each interface may be expressed as [30]

$$k_m\frac{\partial T_m}{\partial r}=k_{m+1}\frac{\partial T_{m+1}}{\partial r}, \qquad (r=R_m) \tag{5}$$

$$T_{m+1}=T_m+k_mZ_m\frac{\partial T_m}{\partial r}, \qquad (r=R_m) \tag{6}$$

for $m=1,2,\ldots,M-1$. Similarly, the following conditions may be written at the interface between the liquid phase and the first layer of encapsulant

$$k_L\frac{\partial T_L}{\partial r}=k_1\frac{\partial T_1}{\partial r}, \qquad (r=R_0) \tag{7}$$

$$T_1=T_L+k_1Z_L\frac{\partial T_1}{\partial r}, \qquad (r=R_0) \tag{8}$$

Finally, the initial temperatures for the liquid phase and encapsulant layers are given by

$$T_m=T_{m,in}(r), \qquad (t=0) \tag{9}$$

$$T_L=T_f, \qquad (t=0) \tag{10}$$

Eqs. (1)–(10) complete the mathematical statement of the multilayer transient thermal conduction problem. Once solved, the resulting temperature distribution may be inserted into the statement of energy conservation at the melting front as follows

$$k_L\left(\frac{\partial T_L}{\partial r}\right)_{r=R_0-a_{LS}}=\rho\mathscr{L}\frac{da_{LS}}{dt} \tag{11}$$

Eq. (11) provides the rate of change of the phase change front at any given time, based on which, the entire phase change front location $a_{LS}(t)$ can be determined through straightforward timestepping. It may be noted that $a_{LS}(t)$ is measured inwards. As a result, the derivative of a_{LS} with respect to time is positive, consistent with the positive sign of the spatial derivative of the temperature field.

The following dimensionless parameters are introduced

$$\xi=\frac{r}{R_0};\chi_{LS}=\frac{a_{LS}}{R_0};\tau=\frac{\alpha_L t}{R_0^2};\theta_m=\frac{T_m-T_f}{T_\infty-T_f};\theta_L=\frac{T_L-T_f}{T_\infty-T_f};\gamma_m=\frac{R_m}{R_0};\bar{\alpha}_m=\frac{\alpha_m}{\alpha_L};\bar{k}_m=\frac{k_m}{k_L};\bar{Z}_m=\frac{k_L Z_m}{R_0};Bi=\frac{hR_0}{k_L};Ste=\frac{C_L\left(T_\infty-T_f\right)}{\mathscr{L}};\theta_{m,in}=\frac{T_{m,in}-T_f}{T_\infty-T_f} \tag{12}$$

where *Ste* and *Bi* are the Stefan and Biot numbers, respectively. The non-dimensional thickness of the m^{th} layer is given by $\gamma_m-\gamma_{m-1}$.

The non-dimensional forms of Eqs. (1)–(11) can be rewritten as follows

$$\frac{1}{\xi}\frac{\partial}{\partial\xi}\left(\xi\frac{\partial\theta_m}{\partial\xi}\right)=\frac{1}{\bar{\alpha}_m}\frac{\partial\theta_m}{\partial\tau},\qquad(\gamma_{m-1}<\xi<\gamma_m,m=1,2,\ldots,M) \tag{13}$$

$$\frac{1}{\xi}\frac{\partial}{\partial\xi}\left(\xi\frac{\partial\theta_L}{\partial\xi}\right)=\frac{\partial\theta_L}{\partial\tau},\qquad(1-\chi_{LS}<\xi<1,m=1,2,\ldots,M) \tag{14}$$

where $\gamma_0=1$.

$$-\bar{k}_M\frac{\partial\theta_M}{\partial\xi}=Bi(\theta_M-1),\qquad(\xi=\gamma_M) \tag{15}$$

$$\theta_L=0,\qquad(\xi=1-\chi_{LS}(\tau)) \tag{16}$$

$$\bar{k}_m\frac{\partial\theta_m}{\partial\xi}=\bar{k}_{m+1}\frac{\partial\theta_{m+1}}{\partial\xi},\qquad(\xi=\gamma_m,m=1,2,\ldots,M-1) \tag{17}$$

$$\theta_{m+1}=\theta_m+\bar{k}_m\bar{Z}_m\frac{\partial\theta_m}{\partial\xi},\qquad(\xi=\gamma_m,m=1,2,\ldots,M-1) \tag{18}$$

$$\frac{\partial\theta_L}{\partial\xi}=\bar{k}_1\frac{\partial\theta_1}{\partial\xi},\qquad(\xi=1) \tag{19}$$

$$\theta_1=\theta_L+\bar{k}_1\bar{Z}_L\frac{\partial\theta_1}{\partial\xi},\qquad(\xi=1) \tag{20}$$

$$\frac{d\chi_{LS}}{d\tau}=Ste\left(\frac{\partial\theta_L}{\partial\xi}\right)_{\xi=1-\chi_{LS}} \tag{21}$$

The non-dimensionalized initial conditions for the encapsulant and liquid phase may be written as

$$\theta_m=\theta_{m,in}(\xi),\qquad(\tau=0) \tag{22}$$

$$\theta_L=0,\qquad(\tau=0) \tag{23}$$

The phase change propagation problem, defined in non-dimensional form by Eqs. (13)–(23) is, in general, a non-linear problem. As is well-known [2–4], exact analytical solutions for phase change problems exist only for very simple problems such as a single-layered PCM. The present case is complicated by the non-melting multilayer encapsulant. In the likely absence of an exact solution for this problem, it is solved using an approximate analytical technique based on transient eigenfunction expansion [14,15,29,31]. Even though the phase change front location changes with time, i.e., $\chi_{LS}=\chi_{LS}(\tau)$, as an approximation, the technique used in this work assumes the temperature field at any time to be given by the solution of a transient thermal conduction problem defined in a domain with fixed boundary χ_{LS}. In other words, at any given time, χ_{LS} is assumed to be stationary and the temperature field is determined by solving the transient thermal conduction problem. This technique is an extension of the well-known quasi-stationary technique [2], which also treats χ_{LS} to be stationary (hence the name quasi-stationary) at any given time and assumes that the temperature distribution is given by the solution of the steady state problem, as opposed to the transient problem in the present work.

Since there is a non-homogenous term in boundary conditions, specifically Eq. (15), the temperature distribution is first split into steady-state and transient components

$$\theta_m(\xi,\tau)=s_m(\xi)+w_m(\xi,\tau) \tag{24}$$

$$\theta_L(\xi,\tau)=s_L(\xi)+w_L(\xi,\tau) \tag{25}$$

where s_m and s_L are the steady-state components, and w_m and w_L are the transient components.

Eqs. (24) and (25) are substituted into Eqs. (13) and (15), respectively, and the transient and steady-state components are separated. Treating the steady state components first, one may write

$$\left(\xi s_m'\right)'=0 \tag{26}$$

$$\left(\xi s_L'\right)'=0 \tag{27}$$

The solutions of Eqs. (26) and (27) are given by

$$s_m=A_m\ln(\xi)+B_m \tag{28}$$

$$s_L=A_L\ln(\xi)+B_L \tag{29}$$

Eqs. (28) and (29) must satisfy boundary conditions as follows

$$-\bar{k}_M s_m'(\gamma_M)=Bi(s_m(\gamma_M)-1) \tag{30}$$

$$s_L(1-\chi_{LS})=0 \tag{31}$$

$$\bar{k}_m s_m'(\gamma_m)=\bar{k}_{m+1}s_{m+1}'(\gamma_m) \tag{32}$$

$$s_{m+1}(\gamma_m)=s_m(\gamma_m)+\bar{k}_m\bar{Z}_m s_m'(\gamma_m) \tag{33}$$

$$s_L'(1)=\bar{k}_1 s_1'(1) \tag{34}$$

$$s_1(1)=s_L(1)+\bar{k}_1\bar{Z}_L s_1'(1) \tag{35}$$

By inserting Eqs. (28) and (29) in Eqs. (30)–(35) and solving the resulting set of linear algebraic equations, the following expressions may be derived for the coefficients

$$A_L=\left[\frac{\ln(\gamma_M)}{\bar{k}_M}-\ln(1-\chi_{LS})+\bar{Z}_L+\frac{1}{Bi\gamma_M}+\left[\sum_{j=1}^{M-1}\left(\frac{1}{\bar{k}_j}-\frac{1}{\bar{k}_{j+1}}\right)\ln(\gamma_j)+\frac{\bar{Z}_j}{\gamma_j}\right]\right]^{-1} \tag{36}$$

$$B_L=-A_L\ln(1-\chi_{LS}) \tag{37}$$

$$A_m=\frac{A_L}{\bar{k}_m},\qquad(m=1,2,\ldots,M) \tag{38}$$

$$B_m=A_L\left[-\ln(1-\chi_{LS})+\bar{Z}_L+\sum_{j=1}^{m-1}\left[\left(\frac{1}{\bar{k}_j}-\frac{1}{\bar{k}_{j+1}}\right)\ln(\gamma_j)+\frac{\bar{Z}_j}{\gamma_j}\right]\right],\ (m=1,2,\ldots,M) \tag{39}$$

The transient components $w_m(\xi,\tau)$ and $w_L(\xi,\tau)$ are solved next. These functions are governed by the following equations

$$\frac{1}{\xi}\frac{\partial}{\partial\xi}\left(\xi\frac{\partial w_m}{\partial\xi}\right)=\frac{1}{\bar{\alpha}_m}\frac{\partial w_m}{\partial\tau},\qquad(\gamma_{m-1}<\xi<\gamma_m,m=1,2,\ldots,M) \tag{40}$$

$$\frac{1}{\xi}\frac{\partial}{\partial\xi}\left(\xi\frac{\partial w_L}{\partial\xi}\right)=\frac{\partial w_L}{\partial\tau},\qquad(1-\chi_{LS}<\xi<1) \tag{41}$$

where all boundary conditions associated with w_m and w_L, similar to Eqs. (15)–(20) are homogeneous as follows

$$-\bar{k}_M\frac{\partial w_M}{\partial\xi}=Bi\cdot w_M,\qquad(\xi=\gamma_M) \tag{42}$$

$$w_L = 0, \qquad (\xi = 1 - \chi_{LS}(\tau)) \tag{43}$$

$$\bar{k}_m \frac{\partial w_m}{\partial \xi} = \bar{k}_{m+1} \frac{\partial w_{m+1}}{\partial \xi}, \qquad (\xi = \gamma_m, m = 1, 2, \ldots, M-1) \tag{44}$$

$$w_{m+1} = w_m + \bar{k}_m \bar{Z}_m \frac{\partial w_m}{\partial \xi}, \qquad (\xi = \gamma_m, m = 1, 2, \ldots, M-1) \tag{45}$$

$$\frac{\partial w_L}{\partial \xi} = \bar{k}_1 \frac{\partial w_1}{\partial \xi}, \qquad (\xi = 1) \tag{46}$$

$$w_1 = w_L + \bar{k}_1 \bar{Z}_L \frac{\partial w_1}{\partial \xi}, \qquad (\xi = 1) \tag{47}$$

and the initial conditions are

$$w_m = \theta_{m,in}(\xi) - s_m(\xi), \qquad (\tau = 0) \tag{48}$$

$$w_L = -s_L(\xi), \qquad (\tau = 0) \tag{49}$$

Eqs. (40) and (41) are solved using the separation of variables method, shown in more detail in Appendix A. This yields

$$w_m(\xi, \tau) = \sum_{n=1}^{\infty} c_n \left(A_{m,n} J_0\left(\frac{\lambda_n \xi}{\sqrt{\bar{\alpha}_m}}\right) + B_{m,n} Y_0\left(\frac{\lambda_n \xi}{\sqrt{\bar{\alpha}_m}}\right) \right) e^{-\lambda_n^2 \tau} \tag{50}$$

$$w_L(\xi, \tau) = \sum_{n=1}^{\infty} c_n \left(A_{L,n} J_0(\lambda_n \xi) + B_{L,n} Y_0(\lambda_n \xi) \right) e^{-\lambda_n^2 \tau} \tag{51}$$

where J_0 and Y_0 are the Bessel functions of first and second kind of order zero, respectively. Using the boundary and interface conditions results in the following set of equations involving the unknown coefficients $A_{m,n}$, $B_{m,n}$, $A_{L,n}$ and $B_{L,n}$ and eigenvalues λ_n

$$\frac{\bar{k}_M}{\sqrt{\bar{\alpha}_M}} \lambda_n J_1\left(\frac{\lambda_n \gamma_M}{\sqrt{\bar{\alpha}_M}}\right) A_{M,n} + \frac{\bar{k}_M}{\sqrt{\bar{\alpha}_M}} \lambda_n Y_1\left(\frac{\lambda_n \gamma_M}{\sqrt{\bar{\alpha}_M}}\right) B_{M,n} = Bi J_0\left(\frac{\lambda_n \gamma_M}{\sqrt{\bar{\alpha}_M}}\right) A_{M,n} + Bi Y_0\left(\frac{\lambda_n \gamma_M}{\sqrt{\bar{\alpha}_M}}\right) B_{M,n} \tag{52}$$

$$\frac{\bar{k}_m}{\sqrt{\bar{\alpha}_m}} \lambda_n J_1\left(\frac{\lambda_n \gamma_m}{\sqrt{\bar{\alpha}_m}}\right) A_{m,n} + \frac{\bar{k}_m}{\sqrt{\bar{\alpha}_m}} \lambda_n Y_1\left(\frac{\lambda_n \gamma_m}{\sqrt{\bar{\alpha}_m}}\right) B_{m,n} = \frac{\bar{k}_{m+1}}{\sqrt{\bar{\alpha}_{m+1}}} \lambda_n J_1\left(\frac{\lambda_n \gamma_m}{\sqrt{\bar{\alpha}_{m+1}}}\right) A_{m+1,n} + \frac{\bar{k}_{m+1}}{\sqrt{\bar{\alpha}_{m+1}}} \lambda_n Y_1\left(\frac{\lambda_n \gamma_m}{\sqrt{\bar{\alpha}_{m+1}}}\right) B_{m+1,n} \tag{53}$$

$$J_0\left(\frac{\lambda_n \gamma_m}{\sqrt{\bar{\alpha}_{m+1}}}\right) A_{m+1,n} + Y_0\left(\frac{\lambda_n \gamma_m}{\sqrt{\bar{\alpha}_{m+1}}}\right) B_{m+1,n} = J_0\left(\frac{\lambda_n \gamma_m}{\sqrt{\bar{\alpha}_m}}\right) A_{m,n} + Y_0\left(\frac{\lambda_n \gamma_m}{\sqrt{\bar{\alpha}_m}}\right) B_{m,n} - \frac{\bar{k}_m \bar{Z}_m}{\sqrt{\bar{\alpha}_m}} \lambda_n J_1\left(\frac{\lambda_n \gamma_m}{\sqrt{\bar{\alpha}_m}}\right) A_{m,n} - \frac{\bar{k}_m \bar{Z}_m}{\sqrt{\bar{\alpha}_m}} \lambda_n Y_1\left(\frac{\lambda_n \gamma_m}{\sqrt{\bar{\alpha}_m}}\right) B_{m,n} \tag{54}$$

$$\lambda_n J_1(\lambda_n) A_{L,n} + \lambda_n Y_1(\lambda_n) B_{L,n} = \frac{\bar{k}_1}{\sqrt{\bar{\alpha}_1}} \lambda_n J_1\left(\frac{\lambda_n}{\sqrt{\bar{\alpha}_1}}\right) A_{1,n} + \frac{\bar{k}_1}{\sqrt{\bar{\alpha}_1}} \lambda_n Y_1\left(\frac{\lambda_n}{\sqrt{\bar{\alpha}_1}}\right) B_{1,n} \tag{55}$$

$$J_0\left(\frac{\lambda_n}{\sqrt{\bar{\alpha}_1}}\right) A_{1,n} + Y_0\left(\frac{\lambda_n}{\sqrt{\bar{\alpha}_1}}\right) B_{1,n} = J_0(\lambda_n) A_{L,n} + Y_0(\lambda_n) B_{L,n} - \frac{\bar{k}_1 \bar{Z}_L}{\sqrt{\bar{\alpha}_1}} \lambda_n J_1\left(\frac{\lambda_n}{\sqrt{\bar{\alpha}_1}}\right) A_{1,n} - \frac{\bar{k}_1 \bar{Z}_L}{\sqrt{\bar{\alpha}_1}} \lambda_n Y_1\left(\frac{\lambda_n}{\sqrt{\bar{\alpha}_1}}\right) B_{1,n} \tag{56}$$

$$J_0(\lambda_n(1-\chi_{LS}))A_{L,n} + Y_0(\lambda_n(1-\chi_{LS}))B_{L,n} = 0 \tag{57}$$

The set of homogeneous equations given by Eqs. (52)–(57) constitutes a non-linear eigenvalue problem. In order to ensure a non-trivial solution for the unknown variables, one must set the determinant Δ of the coefficient matrix to zero. The resulting expression, free of $A_{m,n}$, $B_{m,n}$, $A_{L,n}$ and $B_{L,n}$, constitutes the nonlinear eigenequation, the roots of which are the eigenvalues λ_n of the problem. The eigenequation is cumbersome to write for a general M-layer case, but can easily be derived for simplified cases, such as a single-layered encapsulating wall, as presented in the next section as a special case.

It can be shown [32] that the eigenequation admits an infinite number of roots, λ_n. Since the phase change location χ_{LS} changes with time, therefore, the eigenvalues must be recalculated at each time. This is done by examining successive intervals along the x axis for the plot of the determinant Δ. Considering an interval between x_i and x_{i+1}, the condition $\Delta(x_i)\cdot\Delta(x_{i+1}) < 0$ indicates the presence of a root somewhere in the interval, in which case, the Newton-Raphson method is successively implemented in this interval ten times, resulting in accurate determination of a root. By marching forward in x, a sufficient number of eigenvalues are computed. While this procedure must be repeated at each time, it is not very time-consuming. Each computation of a set of eigenvalues is found to take only a few milliseconds. Further, by using this algorithm to determine the eigenvalues of several standard eigenvalue problems, it is verified that the algorithm does not skip roots or produce spurious eigenvalues.

Once λ_n are determined, one may assign an arbitrary non-zero value to one of the unknown variables, say, $A_{1,n} = 1$. All other coefficients are then determined from Eqs. (52)–(56), where, one of the equations is rendered redundant by the zero determinant requirement.

Finally, the initial conditions given by Eqs. (48) and (49) are used to obtain c_n. Substituting Eqs. (50) and (51) into the initial conditions, Eqs. (48) and (49) results in

$$\theta_{m,in}(\xi) - s_m(\xi) = \sum_{n=1}^{\infty} c_n \left[A_{m,n} J_0\left(\frac{\lambda_n \xi}{\sqrt{\bar{\alpha}_m}}\right) + B_{m,n} Y_0\left(\frac{\lambda_n \xi}{\sqrt{\bar{\alpha}_m}}\right) \right] \tag{58}$$

$$-s_L(\xi) = \sum_{n=1}^{\infty} c_n \left[A_{L,n} J_0(\lambda_n \xi) + B_{L,n} Y_0(\lambda_n \xi) \right] \tag{59}$$

Multiplying both sides of Eq. (58) and (59) by $\frac{\bar{k}_m}{\bar{\alpha}_m}\xi\left[A_{m,n}J_0\left(\frac{\lambda_n\xi}{\sqrt{\bar{\alpha}_m}}\right)+B_{m,n}Y_0\left(\frac{\lambda_n\xi}{\sqrt{\bar{\alpha}_m}}\right)\right]$ and $\xi\left[A_{L,n}J_0(\lambda_n\xi)+B_{L,n}Y_0(\lambda_n\xi)\right]$, respectively, and implementing the principle of quasi-orthogonality [33], one may obtain

$$c_n=\frac{1}{N_n}\left[\sum_{m=1}^{M}\frac{\bar{k}_m}{\bar{\alpha}_m}\int_{\gamma_{m-1}}^{\gamma_m}-s_m(\xi)\left(A_{m,n}J_1\left(\frac{\lambda_n\xi}{\sqrt{\bar{\alpha}_m}}\right)+B_{m,n}Y_1\left(\frac{\lambda_n\xi}{\sqrt{\bar{\alpha}_m}}\right)\right)\xi d\xi+\int_{1-\chi_{LS}}^{1}-s_L(\xi)\left(A_{L,n}J_1(\lambda_n\xi)+B_{L,n}Y_1(\lambda_n\xi)\right)\xi d\xi\right] \tag{60}$$

where

$$N_n=\sum_{m=1}^{M}\frac{\bar{k}_m}{\bar{\alpha}_m}\int_{\gamma_{m-1}}^{\gamma_m}\left(A_{m,n}J_0\left(\frac{\lambda_n\xi}{\sqrt{\bar{\alpha}_m}}\right)+B_{m,n}Y_0\left(\frac{\lambda_n\xi}{\sqrt{\bar{\alpha}_m}}\right)\right)^2\xi d\xi+\int_{1-\chi_{LS}}^{1}\left(A_{L,n}J_0(\lambda_n\xi)+B_{L,n}Y_0(\lambda_n\xi)\right)^2\xi d\xi \tag{61}$$

This completes the derivation of the solution for the transient temperature distribution. By substituting the liquid temperature distribution in Eq. (21), the rate of propagation of the phase change front may be obtained as follows

$$\frac{d\chi_{LS}}{d\tau}=Ste\left(\frac{A_L}{1-\chi_{LS}}-\sum_{n=1}^{\infty}c_n\lambda_n\left(A_{L,n}J_1(\lambda_n(1-\chi_{LS}))-B_{L,n}Y_1(\lambda_n(1-\chi_{LS}))\right)e^{-\lambda_n^2\tau}\right) \tag{62}$$

where J_1 and Y_1 are the Bessel functions of first and second kind of order one, respectively. Thus, at each time that the phase change front location is known, Eq. (62) provides the rate of change of the phase change front location, from where, the entire progression of χ_{LS} with time can be computed recursively, starting with the initial condition. Unfortunately, explicitly integrating Eq. (62) is extremely difficult because, for example, each of the coefficients A_L, B_L, $A_{L,n}$, $B_{L,n}$, c_n as well as the eigenvalues λ_n contain χ_{LS} within themselves. As a result, a numerical integration of Eq. (62), starting with the initial condition $\chi_{LS}(0)=0$ is carried out. Note that an approximation is needed to be made in order to start this recursion at $\tau=0$, since $\chi_{LS}=0$ at $\tau=0$. This is addressed by approximating the propagation of the phase change front over a very short initial time period with the Stefan solution. Provided that this initial time period is very small, this approximation does not significantly affect the predicted phase change front propagation at large times. Once the timestepping begins, the location of the phase change front at any given time is evaluated recursively using the derivative given by Eq. (62), i.e., $\chi_{LS}(\tau+\Delta\tau)=\chi_{LS}(\tau)+\frac{d\chi_{LS}}{d\tau}\Delta\tau$, where $\Delta\tau$ is the timestep and $\frac{d\chi_{LS}}{d\tau}$ is given by Eq. (62).

A key assumption underlying the approximate analytical technique developed in this work is that the phase change front location χ_{LS} is treated to be fixed at any given time, even though, strictly speaking, it is a function of time. This assumption is similar to the well-known quasi-stationary technique[2], which also assumes the phase change front to move slow enough such that a quasi-steady state exists at each time. The assumption underlying the present technique is somewhat less strong, in that instead of completely ignoring transient effects, the transient thermal conduction problem is solved in order to determine the rate of propagation of the phase change front. Regardless, the analytical technique used here is an approximation, and determining the range of non-dimensional parameters over which the method offers reasonable accuracy remains an important question. This is addressed in one of the subsequent sub-sections.

3. Results and discussion

3.1. Special case – homogeneous wall

It is of interest to write the solution for the case of a single-layered wall around the PCM, since a homogeneous wall is encountered in several practical applications. In this case, the temperature distribution in the PCM and wall, as well as the location of the phase change front may be determined by setting $M=1$ in the general results presented in the previous section. It may be shown that the wall and PCM temperature distributions are given by

$$w_1(\xi,\tau)=\left(\frac{\ln(\xi)}{\bar{k}_1}+(\bar{Z}_L-\ln(1-\chi_{LS}))\right)\left(\frac{\ln(\gamma_1)}{\bar{k}_1}-\ln(1-\chi_{LS})+\bar{Z}_L+\frac{1}{Bi\gamma_1}\right)^{-1}+\sum_{n=1}^{\infty}c_n\left(A_{1,n}J_0\left(\frac{\lambda_n\xi}{\sqrt{\bar{\alpha}_1}}\right)+B_{1,n}Y_0\left(\frac{\lambda_n\xi}{\sqrt{\bar{\alpha}_1}}\right)\right)e^{-\lambda_n^2\tau} \tag{63}$$

$$w_L(\xi,\tau)=\ln\left(\frac{\xi}{1-\chi_{LS}}\right)\left(\frac{\ln(\gamma_1)}{\bar{k}_1}-\ln(1-\chi_{LS})+\bar{Z}_L+\frac{1}{Bi\gamma_1}\right)+\sum_{n=1}^{\infty}c_n\left(A_{L,n}J_0(\lambda_n\xi)+B_{L,n}Y_0(\lambda_n\xi)\right)e^{-\lambda_n^2\tau} \tag{64}$$

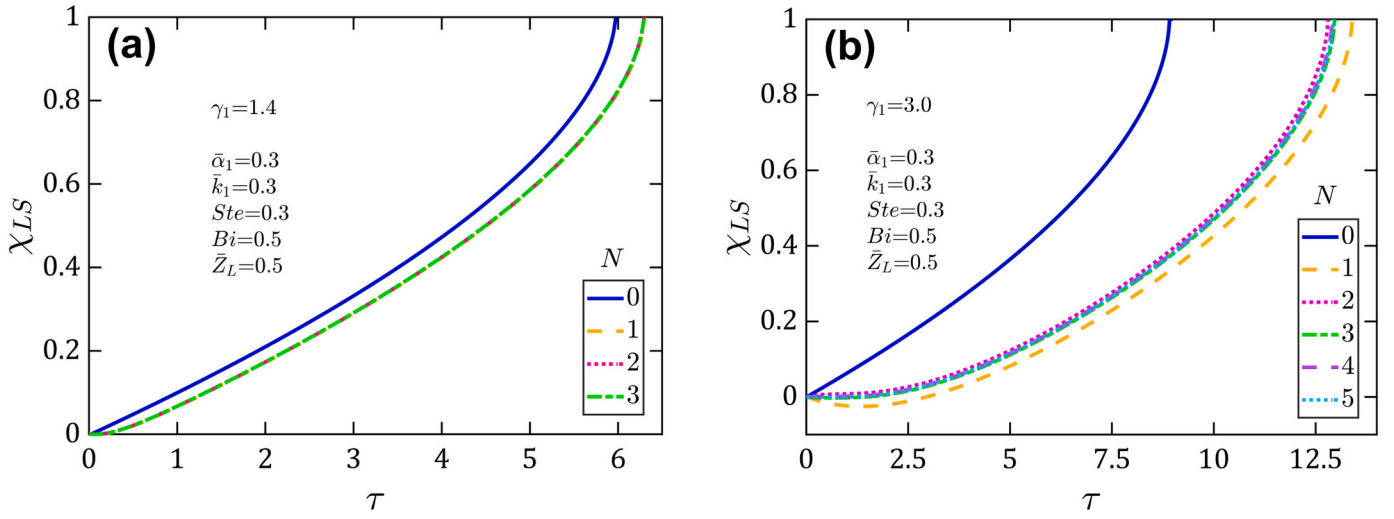

Fig. 2. Effect of number of eigenvalues N: Dimensionless phase change propagation as a function of time with different number of eigenvalues for (a) $\gamma_1 = 1.4$; (b) $\gamma_1 = 3.0$. The case of quasi-steady solution is also included. Values of other parameters are $\bar{\alpha}_1 = 0.3, \bar{k}_1 = 0.3$, $\bar{Z}_L = 0.5$, $Bi = 0.5$, $Ste = 0.3$.

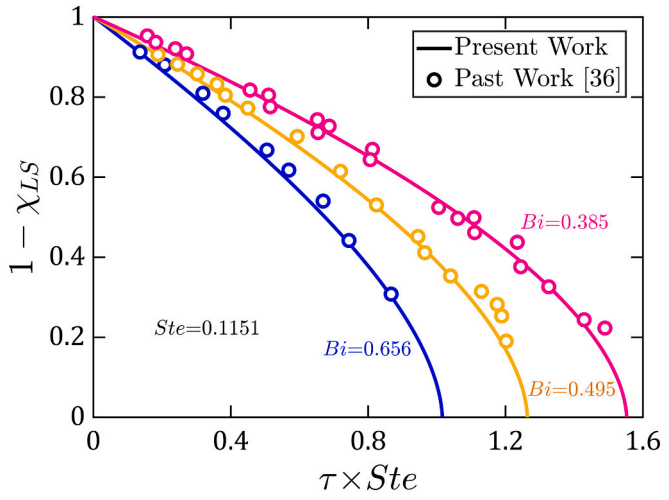

Fig. 3. Comparison with past experimental work by Seban & London [36]: Dimensionless phase change propagation as a function of time for melting of ice without encapsulation ($\gamma_1 = 1$). Comparison is presented for three different values of Bi numbers, as reported by Seban & London [36]. The value of Stefan number is $Ste = 0.1151$.

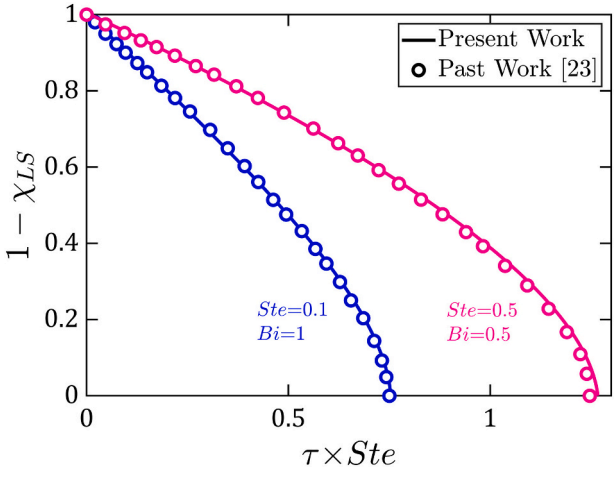

Fig. 4. Comparison with past theoretical model by Shih and Tsay [23]: Dimensionless phase change propagation as a function of time for melting of an PCM without encapsulation ($\gamma_1 = 1$) associated with different values of Bi and Ste.

Subsequently, the propagation of the phase change front is given by

where

$$c_n = \frac{1}{N_n}\left[\frac{\bar{k}_1}{\bar{\alpha}_1}\int_1^{\gamma_1} -s_1(\xi)\left(A_{1,n}J_1\left(\frac{\lambda_n\xi}{\sqrt{\bar{\alpha}_1}}\right)+B_{1,n}Y_1\left(\frac{\lambda_n\xi}{\sqrt{\bar{\alpha}_1}}\right)\right)\xi d\xi + \int_{1-\chi_{LS}}^{1} -\left(\frac{\ln(\xi)}{\bar{k}_1}+(\bar{Z}_L-\ln(1-\chi_{LS}))\right)\left(A_{L,n}J_1(\lambda_n\xi)+B_{L,n}Y_1(\lambda_n\xi)\right)\xi d\xi\right] \tag{65}$$

and

$$N_n = \frac{\bar{k}_1}{\bar{\alpha}_1}\int_1^{\gamma_1}\left(A_{1,n}J_0\left(\frac{\lambda_n\xi}{\sqrt{\bar{\alpha}_1}}\right) + B_{1,n}Y_0\left(\frac{\lambda_n\xi}{\sqrt{\bar{\alpha}_1}}\right)\right)^2\xi d\xi + \int_{1-\chi_{LS}}^{1}\left(A_{L,n}J_0(\lambda_n\xi)+B_{L,n}Y_0(\lambda_n\xi)\right)^2\xi d\xi \tag{66}$$

$$\frac{d\chi_{LS}}{d\tau} = Ste\left(\left[(1-\chi_{LS})\frac{\ln(\gamma_1)}{\bar{k}_1}-\ln(1-\chi_{LS})+\bar{Z}_L + \frac{1}{Bi\gamma_1}\right]^{-1} - \sum_{n=1}^{\infty}c_n\lambda_n\left(A_{L,n}J_1(\lambda_n(1-\chi_{LS}))-B_{L,n}Y_1(\lambda_n(1-\chi_{LS}))\right)e^{-\lambda_n^2\tau}\right) \tag{67}$$

Closed-form expressions for coefficients $A_{1,n}$, $B_{1,n}$, $A_{L,n}$ and $B_{L,n}$

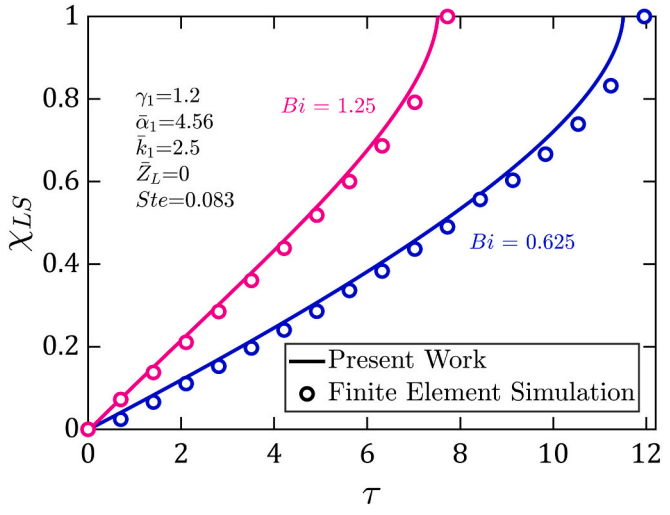

Fig. 5. Comparison with finite-element simulations: Dimensionless phase change propagation versus time for a problem of melting of water surrounded by an annular wall. Curves based on the present work and finite-element simulations are presented for two different values of Biot numbers $Bi = 0.625, 1.25$. Values of other parameters are $\gamma_1 = 1.2$, $\bar{\alpha}_1 = 4.56$, $\bar{k}_1 = 2.5$, $\bar{Z}_L = 0$, $Ste = 0.083$.

appearing in equations above, as well as the eigenequation for this special case are given in Appendix B.

3.2. Effect of number of eigenvalues

Since the solution derived for the temperature distribution and phase change front location are both in the form of infinite series, additional steps need to be taken in order to ensure accuracy. Firstly, the accuracy of the solution depends critically on the computation of the eigenvalues. Accurate computation of eigenvalues is a long-standing challenge [34], for which, a number of root finding techniques are available. In the present case, the *x* axis for the eigenequation is traversed over successive intervals with a fixed step, and, at each point, the product of the values of the eigenequation at the two ends of the step is examined. If the product is negative, the Newton-Raphson method is applied ten times successively in order to obtain a possible root within the interval. This

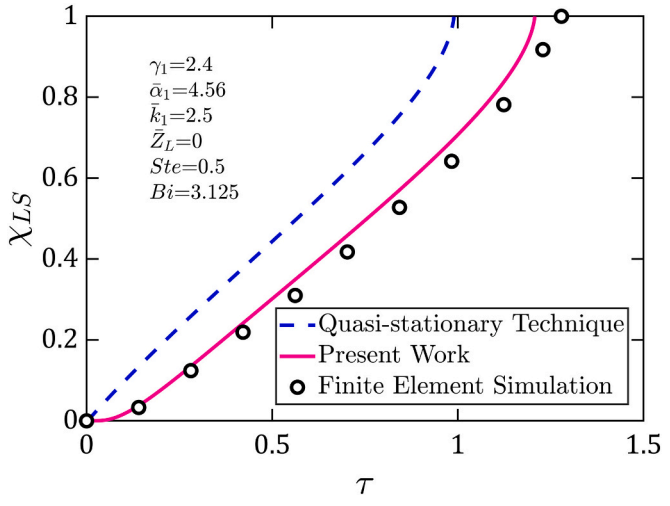

Fig. 6. Comparison of the present work with quasi-stationary technique for moderately large Stefan number. Results from a numerical simulation are also shown for comparison. ($\gamma_1 = 2.4$, $\bar{\alpha}_1 = 0.46$, $\bar{k}_1 = 2.5$, $\bar{Z}_L = 0$, $Ste = 0.5$, $Bi = 3.125$).

algorithm may sometimes identify intervals over which the eigenequation becomes infinite. Such incorrect roots are removed by examining the value of the eigenequation at the candidate value for a root. This technique has been used extensively in past work [14,15].

Further, it is also important to examine the minimum number of roots needed to ensure accuracy within reasonable computational cost. In general, eigenfunction series solutions converge with increasing number of eigenequations, although such convergence may sometimes be very slow [35]. In the present problem, for a representative set of parameters pertaining to a homogeneous encapsulant, the progression of the phase change front is computed using Eq. (67) for increasing number of eigenvalues. Results are plotted in Fig. 2 for two different encapsulant thicknesses. As shown in Fig. 2(a), it is found that for a relatively thin wall, only a small number of eigenvalues are sufficient for series convergence. Even completely neglecting the transient component of the problem, which is equivalent to the well-known quasi-steady technique, results in only around 5% error in terms of the total time for complete melting. On the other hand, for larger wall thickness, as shown in Fig. 2(b), the number of eigenvalues needed for convergence is somewhat larger. In this case, the quasi-steady solution is likely to incur significant error. In general, it is likely that a greater number of eigenvalues will be needed in case of relatively thick, poorly diffusive wall, since the transient component of the solution becomes more and more important under these conditions. In the present problem, the computation of eigenvalues is not computationally challenging, and, therefore, a conservative choice of ten eigenvalues is made for all computations.

3.3. Comparison with past work and numerical simulations

Results from the present work are compared with past papers based on experimental measurements and other analytical techniques for inwards phase change of cylinders. Since past work on an encapsulated cylinder is not available under the assumptions of the present work, therefore, well-known work on homogeneous cylinders is considered as a special case, with a very small value of δ used in the present work for comparison. Fig. 3 presents a comparison with experimental measurements reported by Seban and London [36] for incomplete freezing of water in a copper cylinder cooled by the stream of cold air in a small wind tunnel. Temperatures were measured with a copper-constantan thermocouple and the solidification front location was determined by measuring the mass of ice formed at different times. For three different values of the Biot number *Bi*, Fig. 3 plots the progression of the phase change front. The radial location of the phase change front, $1 - \chi_{LS}(\tau)$ is plotted instead of χ_{LS} in order to be consistent with Seban and London. Each case shows excellent agreement between experimental data and the present work. As expected, the larger the value of the Biot number, the faster is the propagation of the phase change front. Experimental measurement uncertainty from the past work mainly originates in measurement of the frozen layer thickness and calculating convective heat transfer coefficients, whereas key sources of error in the present model include the approximation of the temperature profile with the solution of the transient problem, which is expected to be minimal given the small value of *Ste*, as well as computational errors associated with computing the eigenvalues and integrals involved in computing the norms and coefficients c_n. The good agreement between the present work and experimental data is encouraging.

Additionally, a comparison of the present work with previously reported computation of the inwards melting of a cylinder by Shih and Tsay [23] is carried out. Shih and Tsay computed the frozen layer thickness and temperature distribution for a homogeneous cylinder using the analytical iteration method of Siegel and Savino [37]. Fig. 4 presents this comparison for two different sets of Stefan and Biot numbers. Similar to the comparison with experimental data in Fig. 3, good agreement with past work based on numerical computation is seen in Fig. 4. This establishes further confidence in the accuracy of the present work.

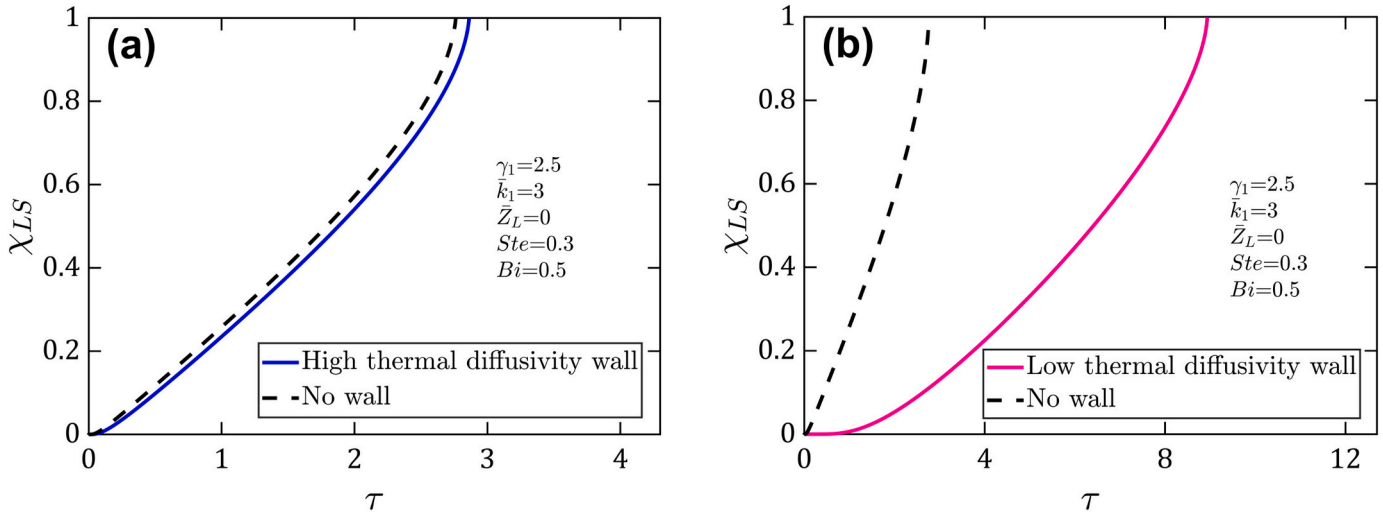

Fig. 7. Importance of accounting for encapsulant wall: Comparison of dimensionless phase change interface location versus time without and with accounting for the presence of the wall. (a) and (b) present results for walls of high diffusivity ($\bar{\alpha}_l = 100$) and low diffusivity ($\bar{\alpha}_l = 0.3$), respectively. Values of other parameters are $\gamma_l = 2.5$, $\bar{k}_l = 3$, $\bar{Z}_L = 0$, $Ste = 0.3$, $Bi = 0.5$.

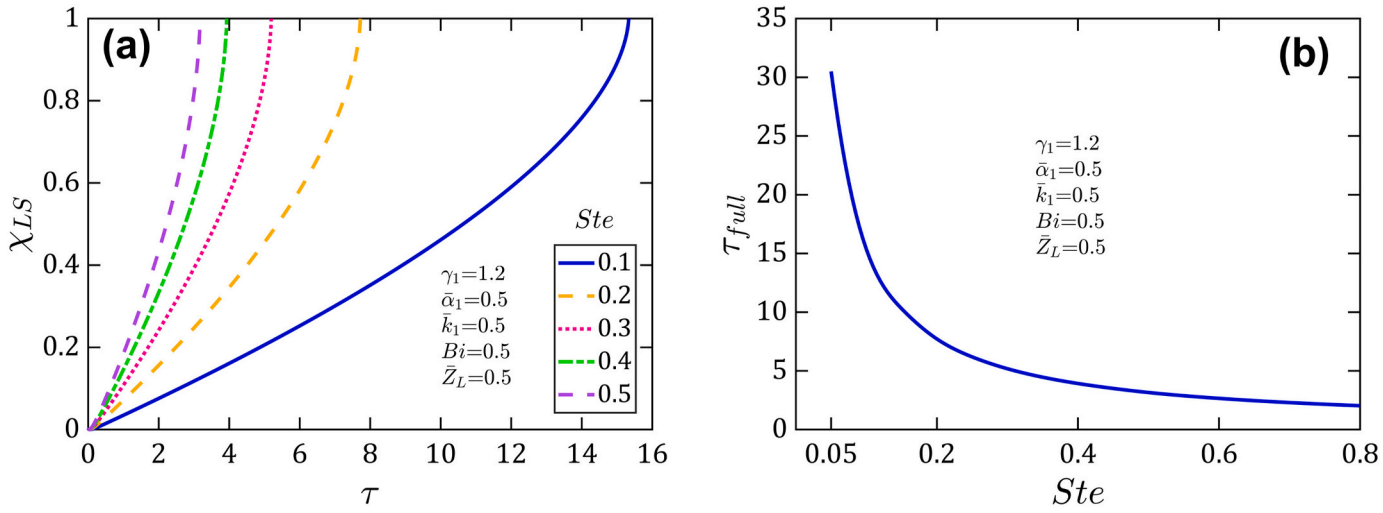

Fig. 8. Effect of Stefan number *Ste*: (a) Dimensionless phase change interface location versus time for different values of *Ste*; (b) Dimensionless complete melting time as a function of *Ste*. Values of other parameters are $\gamma_l = 1.2$, $\bar{\alpha}_l = 0.5$, $\bar{k}_l = 0.5$, $\bar{Z}_L = 0.5$, $Bi = 0.5$.

Finally, comparison of the present work with numerical simulations in a finite-element software is also carried out. For this purpose, the problem of a melting cylinder surrounded by a thick annular region is considered. The top and bottom surfaces are considered to be adiabatic. The dimensionless geometric and thermal properties for this comparison are $\gamma_1 = 1.2, \bar{\alpha}_1 = 4.56, \bar{k}_1 = 2.5, \bar{Z}_L = 0$ and $Ste = 0.083$. For this problem, Fig. 5 presents a comparison between simulation results and the analytical model presented here in terms of the phase change front location as a function of time for two different values of Biot number, $Bi = 0.625$ and 1.25. Both cases are found to show excellent agreement between the analytical model and finite-element simulations, with a worst-case disagreement of <3.8% in the two cases. Note that the present technique compares favorably against numerical simulations in terms of computational time. For a typical phase change problem with a single-layer encapsulant, the entire phase change propagation process is found to be computed using the present work within 2.8 min compared to 162.8 min needed for a finite element based numerical computation using the same timestep on a standard desktop computer (32 GB RAM, 2.6 GHz four-core processor). Moreover, a numerical computation also requires significant time and effort in discretization and typically requires proprietary software.

A comparison of the present work with quasi-stationary technique is presented in Fig. 6. The present work, which tracks the phase change propagation by solving a transient thermal conduction problem may be interpreted as an extension of the quasi-stationary technique, which approximates the temperature field at any time by its steady-state value, s_m and s_L. By accounting for additional transient terms, the accuracy of the present work is expected to be greater than the quasi-stationary technique. For a specific problem, melting curves based on both techniques are presented in Fig. 6, along with results from numerical simulations. The value of Stefan number is reasonably large, $Ste = 0.5$. In such a case, Fig. 6 shows better agreement with simulation results for the present work than the quasi-stationary technique. Thus, the present work offers greater accuracy for moderately large values of *Ste*, at which, the quasi-stationary technique is known to incur significant error [2].

Finally, comparison of the present work with past techniques is carried out in the context of the importance of modeling the encapsulant wall. Most of the past work [23–25,29] on the modeling of inwards

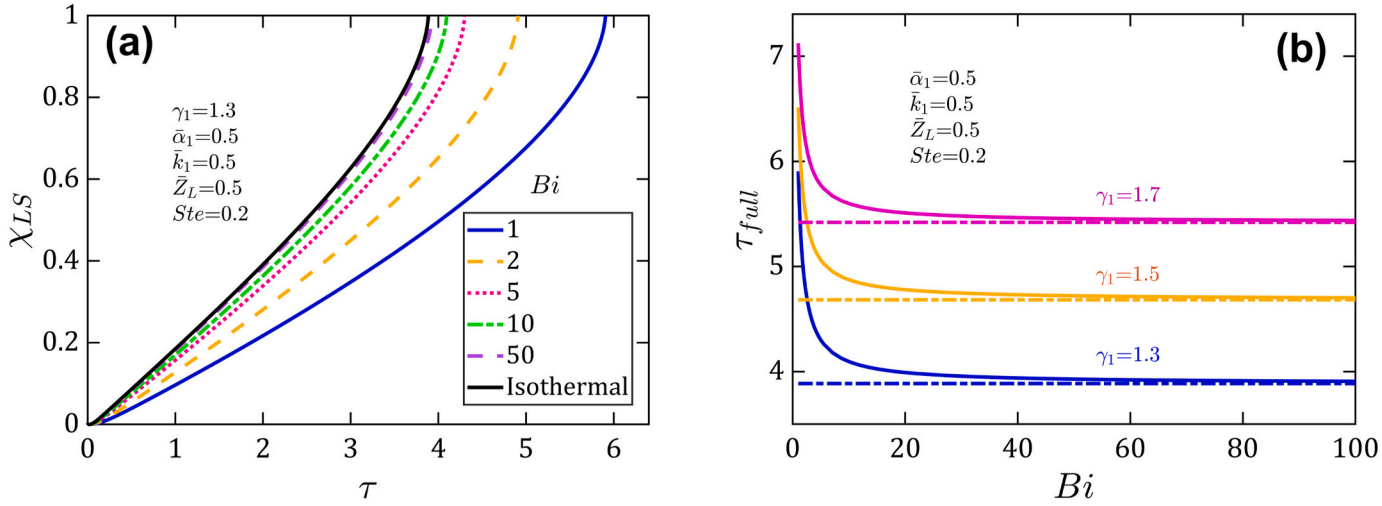

Fig. 9. Effect of Biot number *Bi*: (a) Dimensionless phase change interface location versus time for different values of *Bi* with $\gamma_1 = 1.3$; (b) Dimensionless complete melting time versus *Bi* associated with three different values of encapsulant thickness. The isothermal values of τ_{full} are indicated in (b). Values of other parameters are $\bar{\alpha}_1 = 0.5$, $\bar{k}_1 = 0.5$, $Ste = 0.2$, $\bar{Z}_L = 0.5$.

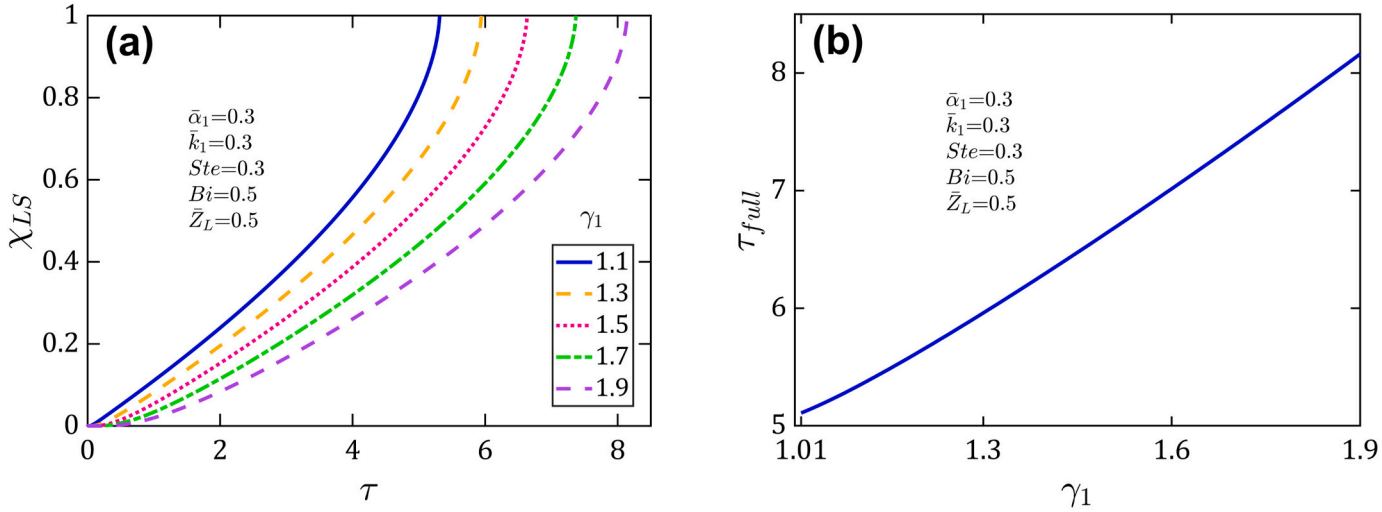

Fig. 10. Effect of encapsulant thickness: (a) Dimensionless phase change interface location versus time for different values of $\bar{\delta}$; (b) Dimensionless complete melting time versus γ_1. Values of other parameters are $\bar{\alpha}_1 = 0.3$, $\bar{k}_1 = 0.3$, $\bar{Z}_L = 0.5$, $Bi = 0.5$, $Ste = 0.3$.

phase change in a cylinder ignores the effect of the encapsulant wall on phase change progression. While doing so may be reasonable when the wall is thin and/or made of highly diffusive material, a thick, poorly diffusive wall is expected to have a signficnat impact on the phase change process, which should not be ignored. In order to illustrate this, Fig. 7 plots the phase change propagation curves for a cylindrical PCM with an annular encapsulant wall. A comparison of results based on the present work is carried out with direct modeling of the phase change process that ignores the presence of the encapsulant wall. Fig. 7(a) and Fig. 7(b) present this comparison for two distinct cases – a highly diffusive wall and a poorly diffusive wall, respectively, while all other problem parameters are held constant. These plots clearly show that relatively small error is incurred in ignoring the presence of the wall, as has been done in past work, when the wall has high thermal diffusivity. This is because in such a case, thermal conduction through the wall occurs rapidly, with minimal impact on the phase change propagation process. In contrast, as shown in Fig. 7(b), ignoring the presence of the wall results in a very inaccurate prediction of the phase change process when the wall is poorly diffusive. In such a case, the presence of the wall leads to significant thermal conduction delay, and, therefore, past techniques that completely ignore the presence of the wall are likely to be in significant error. Instead, the effect of the wall must be properly accounted for, using the technique developed in this work.

3.4. *Effect of externally imposed conditions: Stefan number and Biot number*

The externally imposed conditions that drive inwards propagation of melting in the present problem are represented by the non-dimensional parameters, *Ste* and *Bi*. While *Ste* includes, amongst other parameters, the temperature of the external ambient relative to the melting temperature of the PCM, *Bi* represents the convective heat transfer coefficient that governs convective heat transfer at the external boundary. In general, the larger the value of either the external temperature or the heat transfer coefficient, the faster would be the rate of melting. In order to quantify these expected trends, the propagation of the melting front over time is computed for multiple values of *Ste*, while all other parameters are held constant for a single-layer wall ($\gamma_1 = 1.2, \bar{\alpha}_1 = 0.5$, $\bar{k}_1 = 0.5, \bar{Z}_L = 0.5, Bi = 0.5$). These plots, shown in Fig. 8(a), clearly

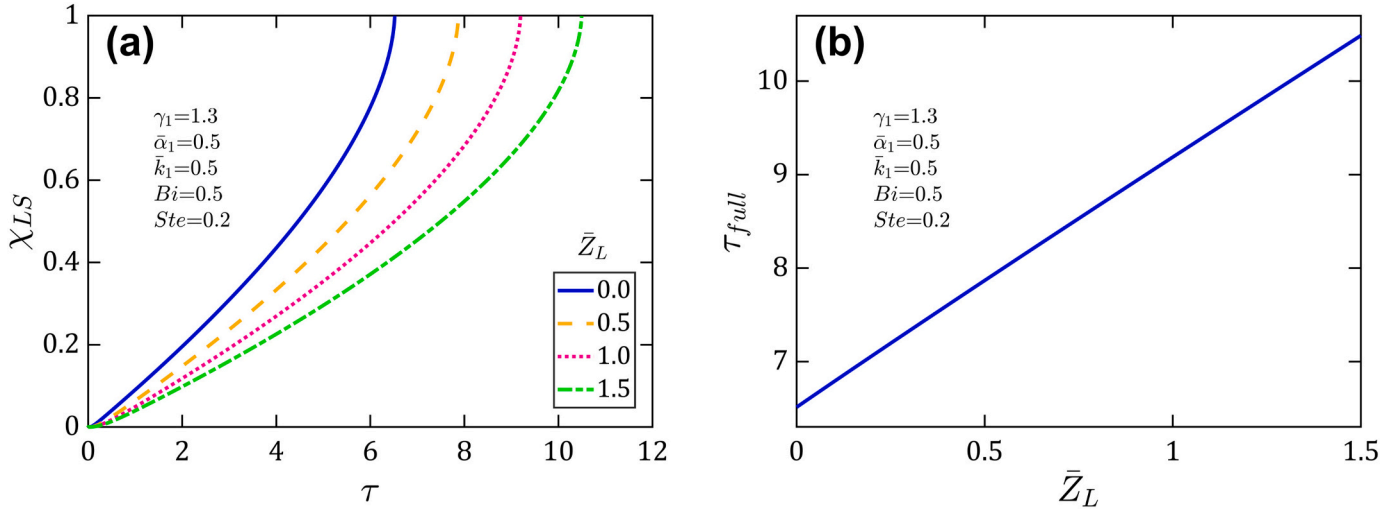

Fig. 11. Effect of thermal contact resistance $\bar{Z}_L$: (a) Dimensionless phase change interface location versus time for different values of $\bar{Z}_L$; (b) Dimensionless complete melting time versus $\bar{Z}_L$. Values of other parameters are $\gamma_1 = 1.3$, $\bar{\alpha}_1 = 0.5$, $\bar{k}_1 = 0.5$, $Ste = 0.2$, $Bi = 0.5$.

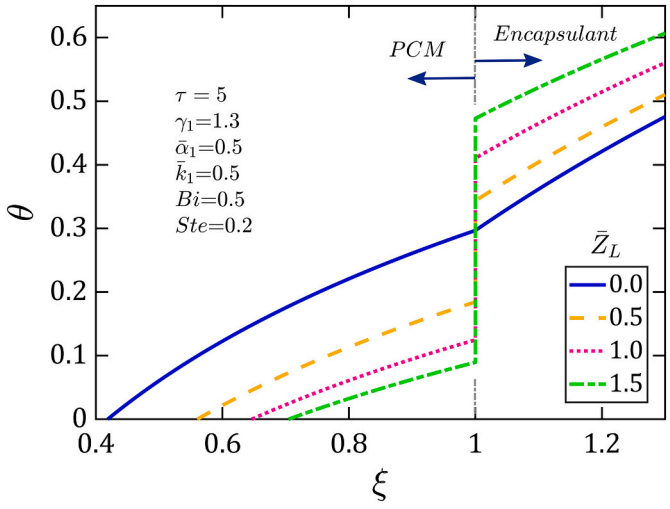

Fig. 12. Dimensionless temperature distribution in the PCM-encapsulant composite at $\tau = 5$ for different values of thermal contact resistance $\bar{Z}_L$. Values of other parameters are $\gamma_1 = 1.3$, $\bar{\alpha}_1 = 0.5$, $\bar{k}_1 = 0.5$, $Ste = 0.2$, $Bi = 0.5$

indicate increased rate of melting with increasing value of Stefan number. This effect is particularly evident for small values of *Ste*. Additionally, the total time taken for full melting of the cylinder, τ_{full} is an important parameter that is often reported in experimental measurements. The dependence of τ_{full} on *Ste* is plotted in Fig. 8(b). It is found that τ_{full} decreases rapidly with increasing *Ste* at first, followed by a saturation effect, wherein τ_{full} continues to decrease, but not as rapidly when *Ste* is relatively larger. This is likely because as *Ste* increases, other factors that contribute to melting, such as diffusion through the wall and the liquid phase become more and more dominant.

The effect of *Bi* is investigated next. Similar to Fig. 8, melting front propagation curves are plotted for different values of *Bi*, while other parameters are held constant ($\bar{\alpha}_1 = 0.5, \bar{k}_1 = 0.5, Ste = 0.2, \bar{Z}_L = 0.5$). The limiting case of an isothermal boundary condition is also shown. As expected, increasing the Biot number results in faster propagation of the melting front, which is because of increased convective heat transfer into the encapsulant. As expected, curves in Fig. 9 exhibit a saturation effect, in that at sufficiently large value of *Bi*, further increasing its value does not cause a significant change in the melting curve. This is because a sufficiently large value of *Bi*, around $Bi = 50$ in this case, is close enough to the isothermal boundary condition, and there is no significant change incurred by further increasing *Bi*. The time taken for full melting is plotted as a function of *Bi* in Fig. 9(b). Three different cases of the encapsulant thickness are considered. In each case, the corresponding limit for the isothermal boundary condition, computed separately is also shown. Consistent with expectations, Fig. 9(b) shows that the larger the value of *Bi*, the shorter is the time taken for full melting. The saturation effect associated with approaching the isothermal limit is seen at around $Bi = 50$ in each case, consistent with the melting curves in Fig. 9(a). As expected, the curves in Fig. 9(b) for different encapsulant thickness show increased time for melting with increasing encapsulant thickness. This is simply due to the greater resistance to heat flow offered by a thicker wall.

3.5. Effect of encapsulant thickness

As indicated in Fig. 9(b), the encapsulant thickness plays an important role in determining the melting characteristics since it determines the rate of heat transfer across the wall. The impact of the wall thickness is investigated further in Fig. 10. Phase change propagation as a function of time is plotted for multiple wall thicknesses in Fig. 10(a), whereas the time taken for full melting is plotted as a function of γ_1 in Fig. 10(b). These plots quantify the impact of the wall thickness. Fig. 10(a) shows, for example, as expected, a slowdown in the melting front curve as the wall thickness increases. Unlike the saturation effects observed in connection with the Stefan number and Biot number in the previous subsection, the effect of the wall thickness on the melting process is nearly linear – the thicker the wall, the longer it takes for the melting process to finish, as shown in Fig. 10(b).

3.6. Effect of thermal contact resistance

A key feature of the theoretical model presented here is that the effect of thermal contact resistance at interfaces is accounted for. The thermal contact resistance appears, for example, in the eigenequation. From a practical perspective, it is of interest to determine how the thermal contact resistance affects the melting process. It is expected that a large thermal contact resistance will slow down thermal conduction from the outer boundary towards the melting front and, therefore, slow down the melting process. This is quantified in Fig. 11(a), where the phase change propagation as a function of time is plotted for multiple

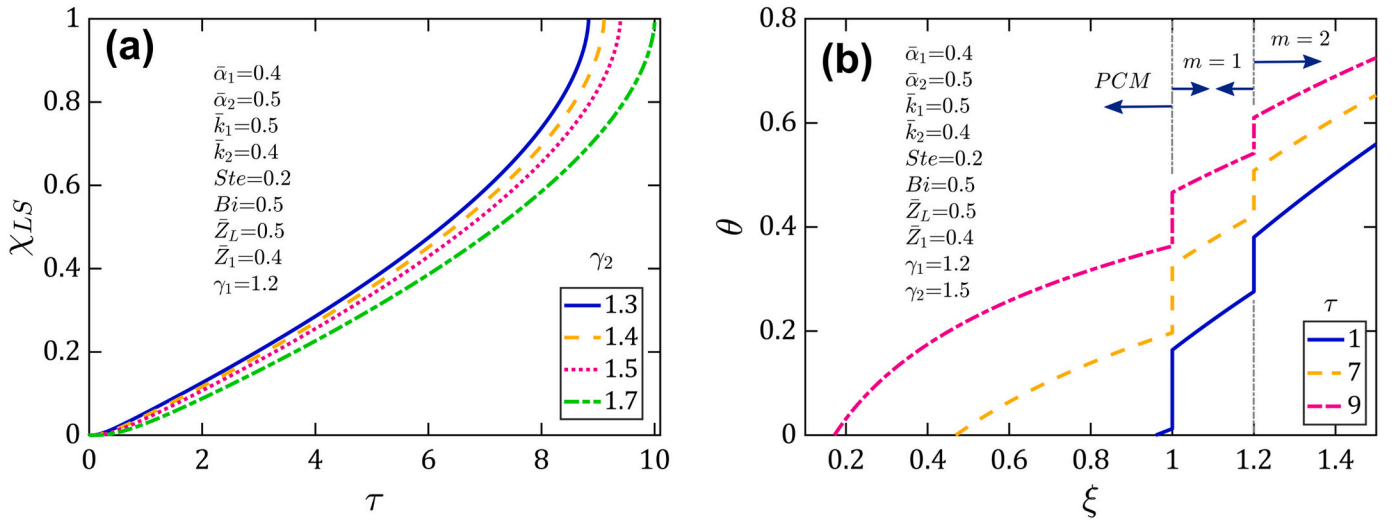

Fig. 13. Phase change propagation and temperature distribution for a two-layered encapsulant: (a) Dimensionless phase change interface location versus time for different values of γ_2 with $\gamma_1 = 1.2$; (b) Dimensionless temperature distribution in the PCM-encapsulant composite with two layers of encapsulant at different times for $\gamma_1 = 1.2$ and $\gamma_2 = 1.5$. Values of other parameters are $\bar{\alpha}_1 = 0.4$, $\bar{\alpha}_2 = 0.5, \bar{k}_1 = 0.5$, $\bar{k}_2 = 0.4$, $Ste = 0.2$, $Bi = 0.5$, $\bar{Z}_L = 0.5$, $\bar{Z}_1 = 0.4$.

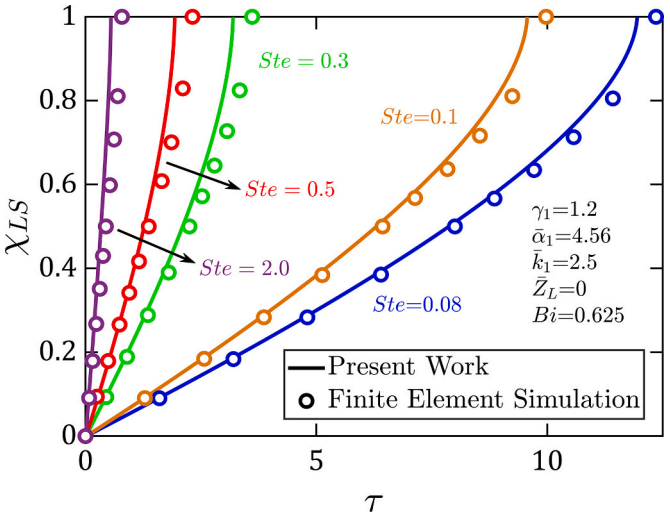

Fig. 14. Error as a function of Stefan number: Comparison of the approximate technique developed here with finite-element simulations in terms of phase change propagation curves at multiple values of *Ste*. Other problem parameters are $\gamma_1 = 1.2$, $\bar{\alpha}_1 = 4.56$, $\bar{k}_1 = 2.5$, $\bar{Z}_L = 0$, $Bi = 0.625$.

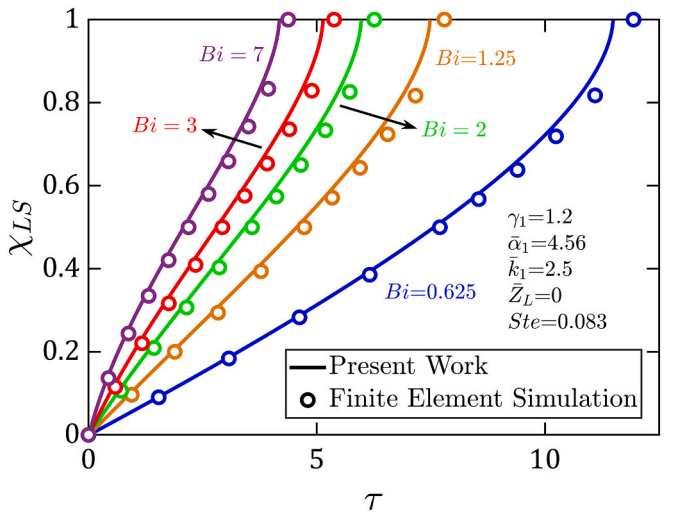

Fig. 15. Error as a function of Biot number: Comparison of the approximate technique developed here with finite-element simulations in terms of phase change propagation curves at multiple values of *Bi*. Other problem parameters are $\gamma_1 = 1.2, \bar{\alpha}_1 = 4.56, \bar{k}_1 = 2.5, \bar{Z}_L = 0, Ste = 0.083$.

Table 1
Comparison of prediction of time taken for 50% completion of melting by the present work and numerical simulations for multiple values of *Ste*. The % error between the two is also listed.

Ste	$\tau_{1/2}$		% Error
	Present Work	Simulations	
0.05	12.59	12.71	0.91
0.08	7.87	8.00	1.61
0.1	6.31	6.43	1.93
0.3	2.10	2.25	6.50
0.5	1.27	1.37	7.03
0.8	0.81	0.91	10.96
1.0	0.65	0.73	11.46
1.5	0.43	0.55	21.56
2.0	0.34	0.44	23.82
3.0	0.24	0.33	25.85

Table 2
Comparison of prediction of time taken for 50% completion of melting by the present work and numerical simulations for multiple values of *Bi*. The % error between the two is also listed.

Bi	$\tau_{1/2}$		% Error
	Present Work	Simulations	
0.3	14.11	14.24	0.96
0.625	7.57	7.70	1.63
1.25	4.57	4.73	3.36
2.0	3.44	3.58	4.08
2.5	3.06	3.19	4.20
3.0	2.81	2.93	4.26
4.0	2.50	2.62	4.39
5.0	2.31	2.42	4.57
6.0	2.19	2.29	4.66
7.0	2.09	2.20	4.74

values of the contact resistance at the PCM-wall interface. The limiting case of perfect contact ($\bar{Z}_L = 0$) is also shown. As expected, the melting process slows down with increasing $\bar{Z}_L$, which is also observed in the dependence of τ_{full} on $\bar{Z}_L$, shown in Fig. 11(b). Similar to the effect of the wall thickness, the effect of $\bar{Z}_L$ on τ_{full} is also linear. This may arise from the fact that both wall thickness and $\bar{Z}_L$ offer linear resistance to the flow of heat across the wall and into the PCM.

The impact of $\bar{Z}_L$ on the temperature distribution in this problem is further shown in Fig. 12, which plots the temperature distributions at a specific time in both PCM and wall for different values of $\bar{Z}_L$. A continuous temperature curve is observed at the interface for the limiting case of perfect thermal contact, whereas a temperature discontinuity is observed for all other cases of non-zero $\bar{Z}_L$. As expected, the greater the contact resistance, the greater is the temperature drop across the interface.

3.7. Phase change in a two-layered encapsulant

While most of the analysis presented above considered a single-layered annular encapsulant around the PCM core, the model presented in Section 2 is quite general and capable of accounting for an arbitrary number of encapsulant layers. In order to demonstrate this, phase change propagation is analyzed for the case of a two-layered encapsulant. Fig. 13(a) presents phase change propagation as a function of time for four different values of the relative thickness of the outer encapsulant layer. The general behavior of χ_{LS} as a function of τ is similar to previous plots, and there is some dependence on the thickness of the outer encapsulant. As expected, the larger this thickness, the slower is the progression of the melting front. Fig. 13(b) plots temperature distributions in the three-layer geometry comprising the PCM core and the two encapsulant layers at three different times. The left-wards progression of the temperature curves in this plot indicates outwards propagation of the melting front, with the melting process about 80% complete at $\tau = 9$. The discontinuity in the temperature curves at interfaces in Fig. 13(b) is due to the non-zero interfacial thermal contact resistance. While the computation cost associated with a multi-layer encapsulant increases with increasing number of layers, nevertheless, Section 2 completely outlines the final results for temperature distribution and phase change front propagation for a general case, which is quite straightforward to compute, even for a large number of layers.

3.8. Accuracy of the approximate technique

The technique developed in this work is inherently approximate, due to the assumption that the temperature distribution at any time is given by the solution of a transient multilayer thermal conduction problem with fixed phase change front, which results in an expression for the rate of propagation of the melting process. The approximate nature of the technique is not entirely surprising, since phase change problems are known to be non-linear in nature [2], and exact solutions are available only for the simplest phase change problems, such as one without an encapsulant and a constant temperature boundary condition in a Cartesian geometry. Given the approximate nature of the solution developed here, however, it is important to quantify the extent of error incurred, and, in particular, identify the range of key non-dimensional parameters, over which, reasonable accuracy may be expected.

Towards this, the error incurred in this technique compared to finite-element simulations is determined as a function of two key non-dimensional parameters – *Ste* and *Bi*. Firstly, for a representative problem, Fig. 14 plots phase change front location as a function of time for multiple values of *Ste*. In each case, results from the present work are compared with finite-element numerical simulations. In addition, the % error between the present work and finite-element simulations for each *Ste* is listed in Table 1. Note that the % error is computed in terms of $\tau_{1/2}$, the time taken to reach 50% completion of the melting process, i.e., $\chi_{LS} = 0.5$. Fig. 14 shows reasonably good agreement between the two, particularly at low *Ste*, which is to be expected due to the slow rate of propagation of phase change at low *Ste*. As *Ste* increases, Fig. 14 shows greater relative deviation between the two, also quantified by the % error data shown in Table 1. These data show that in order for the approximate technique developed here to be within 10% accuracy, the value of *Ste* should be below 0.9. If a greater error, say 20%, is tolerable, then up to $Ste = 1.5$ is acceptable. This analysis quantifies the range of *Ste*, over which, the method discussed in this work offers reasonable accuracy.

Similarly, the impact of *Bi* on accuracy of the approximate method is investigated in Fig. 15, in which, the present work is compared with finite-element simulations in terms of phase change front location as a function of time for multiple values of *Bi*. In addition, the % error between the present work and finite-element simulations for each *Bi* is listed in Table 2. Unlike the impact of *Ste*, Fig. 15 and Table 2 show that the error incurred in the approximate method developed here is largely insensitive to the Biot number. This may be mainly due to the relative lack of impact of *Bi* on the rate of propagation of the melting process, which governs the accuracy of the key approximation made in this work.

4. Conclusions

The key contribution of this work is in the development of an approximate analytical technique based on series expansion to predict the rate of phase change in a cylindrical PCM when surrounded by a multilayer wall. This accounts for an important practical consideration, whereas most of the past work has assumed direct melting of the PCM. By correctly accounting for thermal conduction through the wall, the model developed here is likely to be a lot more accurate in realistic conditions.

It is important to note the key assumptions made to simplify analysis in this work. Natural convection in the melted liquid has been neglected, and all properties are assumed to be constant. Both of these assumptions are likely to be reasonable when the temperature range is not particularly large. A quantitative assessment of the accuracy of such assumptions in the context of a given problem may be carried out, for example, by calculating the Rayleigh number. Additionally, a single-valued melting temperature is assumed here, rather than a material that melts over a temperature range. The initial phase, solid in this case, is assumed to be initially at the melting temperature, which is a reasonable assumption, but can easily be relaxed by accounting for heat transfer into the solid phase through an additional layer in the multilayer problem solved here. Finally, it must be noted that the transient eigenfunction expansion technique used here is an approximate one, as it assumes the temperature distribution at any time to be given by the solution of a fixed boundary transient thermal conduction problem. Exact solutions for phase change problems are unlikely, and approximate methods such as the one presented here are useful for analysis. In the present case, good accuracy may be expected for low and moderate values of the Stefan number.

This work expands the state-of-the-art in theoretical analysis of phase change heat transfer, particularly for multilayer bodies. Results and insights gained from this work may help in the design and optimization of a variety of thermal management, energy storage and other related systems.

CRediT authorship contribution statement

Emad Hasrati: Methodology, Formal analysis, Validation, Data curation, Writing – original draft, Writing – review & editing. **Ankur Jain:** Conceptualization, Methodology, Formal analysis, Project administration, Writing – original draft, Writing – review & editing.

Declaration of Competing Interest

All authors hereby declare that they do not have any conflicts of interest in connection with the material presented here.

Data availability

Data will be made available on request.

Appendix A. Solution of the transient components

To begin with, eqs. (40) and (41) are reproduced below:

$$\frac{1}{\xi}\frac{\partial}{\partial\xi}\left(\xi\frac{\partial w_m}{\partial\xi}\right)=\frac{1}{\bar{\alpha}_m}\frac{\partial w_m}{\partial\tau},\qquad(\gamma_{m-1}<\xi<\gamma_m, m=1,2,\ldots,M) \tag{A.1}$$

$$\frac{1}{\xi}\frac{\partial}{\partial\xi}\left(\xi\frac{\partial w_L}{\partial\xi}\right)=\frac{\partial w_L}{\partial\tau},\qquad(1-\chi_{LS}<\xi<1) \tag{A.2}$$

Based on the separation of variables technique, it may be assumed that

$$w_m(\xi,\tau)=f_m(\xi)g_m(\tau) \tag{A.3}$$

$$w_L(\xi,\tau)=f_L(\xi)g_L(\tau) \tag{A.4}$$

Substituting Eqs. (A.3) and (A.4) into Eqs. (A.1) and (A.2), respectively, one may obtain

$$\frac{1}{\xi}\left(\xi f_m^{'}g_m\right)^{'}=\frac{1}{\bar{\alpha}_m}f_m g_m \tag{A.5}$$

$$\frac{1}{\xi}\left(\xi f_L^{'}g_L\right)^{'}=f_L g_L \tag{A.6}$$

Eq. (A.5) may be recast as

$$\xi^2 f_m^{''}+\xi f_m+\frac{\lambda_n^2}{\bar{\alpha}_m}\xi^2 f_m=0 \tag{A.7}$$

$$g_m^{'}+\lambda_n^2 g_m=0 \tag{A.8}$$

and Eq. (A.6) may be recast as

$$\xi^2 f_L^{''}+\xi f_L+\lambda_n^2\xi^2 f_L=0 \tag{A.9}$$

$$g_L^{'}+\lambda_n^2 g_L=0 \tag{A.10}$$

Eqs. (A.8) and (A.10) admit exponential terms for the time-dependent component, whereas, for the spatial component, Eqs. (A.7) and (A.9), the solution involves Bessel equations. Combining the two in an infinite series results in the solution in the form given by Eqs. (50) and (51).

Appendix B. Closed-form expressions for the special case in Section 3.1

This Appendix presents expressions for coefficients $A_{1,n}$, $B_{1,n}$, $A_{L,n}$ and $B_{L,n}$ appearing in Eqs. (63)–(67) as well as the eigenequation for the special case of single-layered wall problem.

By setting $A_{1,n}=1$, one may find $B_{1,n}$, $A_{L,n}$, $B_{L,n}$ from the boundary and interface conditions as

$$\frac{B_{1,n}=-\frac{\bar{k}_1}{\sqrt{\bar{\alpha}_1}}\lambda_n J_1\left(\frac{\lambda_n\gamma_1}{\sqrt{\bar{\alpha}_1}}\right)-BiJ_0\left(\frac{\lambda_n\gamma_1}{\sqrt{\bar{\alpha}_1}}\right)}{\frac{\bar{k}_1}{\sqrt{\bar{\alpha}_1}}\lambda_n Y_1\left(\frac{\lambda_n\gamma_1}{\sqrt{\bar{\alpha}_1}}\right)-BiY_0\left(\frac{\lambda_n\gamma_1}{\sqrt{\bar{\alpha}_1}}\right)} \tag{B.1}$$

$$\begin{aligned}A_{L,n}=\Bigg[&\frac{\bar{k}_1}{\sqrt{\bar{\alpha}_1}}Y_0(\lambda_n)Y_1\left(\frac{\lambda_n}{\sqrt{\bar{\alpha}_1}}\right)\left(BiJ_0\left(\frac{\lambda_n\gamma_1}{\sqrt{\bar{\alpha}_1}}\right)-\frac{\bar{k}_1}{\sqrt{\bar{\alpha}_1}}\lambda_n J_1\left(\frac{\lambda_n\gamma_1}{\sqrt{\bar{\alpha}_1}}\right)\right)+\frac{\bar{k}_1}{\sqrt{\bar{\alpha}_1}}Y_0(\lambda_n)J_1\left(\frac{\lambda_n}{\sqrt{\bar{\alpha}_1}}\right)\left(\frac{\bar{k}_1}{\sqrt{\bar{\alpha}_1}}\lambda_n Y_1\left(\frac{\lambda_n\gamma_1}{\sqrt{\bar{\alpha}_1}}\right)\right.\\&\left.-BiY_0\left(\frac{\lambda_n\gamma_1}{\sqrt{\bar{\alpha}_1}}\right)\right)+Y_1(\lambda_n)\left(\frac{\bar{k}_1}{\sqrt{\bar{\alpha}_1}}\lambda_n J_1\left(\frac{\lambda_n\gamma_1}{\sqrt{\bar{\alpha}_1}}\right)\right.\\&\left.-BiJ_0\left(\frac{\lambda_n\gamma_1}{\sqrt{\bar{\alpha}_1}}\right)\right)\left(Y_0\left(\frac{\lambda_n}{\sqrt{\bar{\alpha}_1}}\right)+\frac{\bar{k}_1\bar{Z}_L}{\sqrt{\bar{\alpha}_1}}\lambda_n Y_1\left(\frac{\lambda_n}{\sqrt{\bar{\alpha}_1}}\right)\right)+Y_1(\lambda_n)\left(J_0\left(\frac{\lambda_n}{\sqrt{\bar{\alpha}_1}}\right)+\frac{\bar{k}_1\bar{Z}_L}{\sqrt{\bar{\alpha}_1}}\lambda_n J_1\left(\frac{\lambda_n}{\sqrt{\bar{\alpha}_1}}\right)\right)\left(BiY_0\left(\frac{\lambda_n\gamma_1}{\sqrt{\bar{\alpha}_1}}\right)-\frac{\bar{k}_1}{\sqrt{\bar{\alpha}_1}}\lambda_n Y_1\left(\frac{\lambda_n\gamma_1}{\sqrt{\bar{\alpha}_1}}\right)\right)\Bigg]\Bigg[(J_1(\lambda_n)Y_0(\lambda_n)\\&-J_0(\lambda_n)Y_1(\lambda_n))\left(\frac{\bar{k}_1}{\sqrt{\bar{\alpha}_1}}\lambda_n Y_1\left(\frac{\lambda_n\gamma_1}{\sqrt{\bar{\alpha}_1}}\right)\right.\\&\left.-BiY_0\left(\frac{\lambda_n\gamma_1}{\sqrt{\bar{\alpha}_1}}\right)\right)\Bigg]^{-1}\end{aligned} \tag{B.2}$$

$$B_{L,n}=\left[\frac{\bar{k}_1}{\sqrt{\bar{\alpha}_1}}Y_1\left(\frac{\lambda_n}{\sqrt{\bar{\alpha}_1}}\right)J_0(\lambda_n)\left(\frac{\bar{k}_1}{\sqrt{\bar{\alpha}_1}}\lambda_n J_1\left(\frac{\lambda_n\gamma_1}{\sqrt{\bar{\alpha}_1}}\right)-BiJ_0\left(\frac{\lambda_n\gamma_1}{\sqrt{\bar{\alpha}_1}}\right)\right)+\frac{\bar{k}_1}{\sqrt{\bar{\alpha}_1}}J_0(\lambda_n)J_1\left(\frac{\lambda_n}{\sqrt{\bar{\alpha}_1}}\right)\left(\frac{\bar{k}_1}{\sqrt{\bar{\alpha}_1}}\lambda_n Y_1\left(\frac{\lambda_n\gamma_1}{\sqrt{\bar{\alpha}_1}}\right)-BiY_0\left(\frac{\lambda_n\gamma_1}{\sqrt{\bar{\alpha}_1}}\right)\right)+J_1(\lambda_n)\left(\frac{\bar{k}_1}{\sqrt{\bar{\alpha}_1}}\lambda_n J_1\left(\frac{\lambda_n\gamma_1}{\sqrt{\bar{\alpha}_1}}\right)-BiJ_0\left(\frac{\lambda_n\gamma_1}{\sqrt{\bar{\alpha}_1}}\right)\right)\left(Y_0\left(\frac{\lambda_n}{\sqrt{\bar{\alpha}_1}}\right)+\frac{\bar{k}_1\bar{Z}_L}{\sqrt{\bar{\alpha}_1}}\lambda_n Y_1\left(\frac{\lambda_n}{\sqrt{\bar{\alpha}_1}}\right)\right)-J_1(\lambda_n)\left(J_0\left(\frac{\lambda_n}{\sqrt{\bar{\alpha}_1}}\right)+\frac{\bar{k}_1\bar{Z}_L}{\sqrt{\bar{\alpha}_1}}\lambda_n J_1\left(\frac{\lambda_n}{\sqrt{\bar{\alpha}_1}}\right)\right)\left(\frac{\bar{k}_1}{\sqrt{\bar{\alpha}_1}}\lambda_n Y_1\left(\frac{\lambda_n\gamma_1}{\sqrt{\bar{\alpha}_1}}\right)-BiY_0\left(\frac{\lambda_n\gamma_1}{\sqrt{\bar{\alpha}_1}}\right)\right)\right]\left[\left(\frac{\bar{k}_1}{\sqrt{\bar{\alpha}_1}}\lambda_n Y_1\left(\frac{\lambda_n\gamma_1}{\sqrt{\bar{\alpha}_1}}\right)-BiY_0\left(\frac{\lambda_n\gamma_1}{\sqrt{\bar{\alpha}_1}}\right)\right)\left(J_1(\lambda_n)Y_0(\lambda_n)-J_0(\lambda_n)Y_1(\lambda_n)\right)\right]^{-1} \tag{B.3}$$

Additionally, the eigenequation for this problem is derived as follows:

$$-\left[J_0(\lambda_n)Y_0(\lambda_n(1-\chi_{LS}))\frac{\bar{k}_1}{\sqrt{\bar{\alpha}_1}}Y_1\left(\frac{\lambda_n}{\sqrt{\bar{\alpha}_1}}\right)\left(\frac{\bar{k}_1}{\sqrt{\bar{\alpha}_1}}\lambda_n J_1\left(\frac{\lambda_n\gamma_1}{\sqrt{\bar{\alpha}_1}}\right)-BiJ_0\left(\frac{\lambda_n\gamma_1}{\sqrt{\bar{\alpha}_1}}\right)\right)\right]+\left[\frac{\bar{k}_1}{\sqrt{\bar{\alpha}_1}}Y_1\left(\frac{\lambda_n}{\sqrt{\bar{\alpha}_1}}\right)J_0(\lambda_n(1-\chi_{LS}))Y_0(\lambda_n)\left(\frac{\bar{k}_1}{\sqrt{\bar{\alpha}_1}}\lambda_n J_1\left(\frac{\lambda_n\gamma_1}{\sqrt{\bar{\alpha}_1}}\right)-BiJ_0\left(\frac{\lambda_n\gamma_1}{\sqrt{\bar{\alpha}_1}}\right)\right)\right]+\left[J_0(\lambda_n)\frac{\bar{k}_1}{\sqrt{\bar{\alpha}_1}}J_1\left(\frac{\lambda_n}{\sqrt{\bar{\alpha}_1}}\right)Y_0(\lambda_n(1-\chi_{LS}))\left(\frac{\bar{k}_1}{\sqrt{\bar{\alpha}_1}}\lambda_n Y_1\left(\frac{\lambda_n\gamma_1}{\sqrt{\bar{\alpha}_1}}\right)-BiY_0\left(\frac{\lambda_n\gamma_1}{\sqrt{\bar{\alpha}_1}}\right)\right)\right]-\left[\frac{\bar{k}_1}{\sqrt{\bar{\alpha}_1}}J_1\left(\frac{\lambda_n}{\sqrt{\bar{\alpha}_1}}\right)J_0(\lambda_n(1-\chi_{LS}))Y_0(\lambda_n)\left(\frac{\bar{k}_1}{\sqrt{\bar{\alpha}_1}}\lambda_n Y_1\left(\frac{\lambda_n\gamma_1}{\sqrt{\bar{\alpha}_1}}\right)-BiY_0\left(\frac{\lambda_n\gamma_1}{\sqrt{\bar{\alpha}_1}}\right)\right)\right]+\left[J_1(\lambda_n)Y_0(\lambda_n(1-\chi_{LS}))\left(\frac{\bar{k}_1}{\sqrt{\bar{\alpha}_1}}\lambda_n J_1\left(\frac{\lambda_n\gamma_1}{\sqrt{\bar{\alpha}_1}}\right)-BiJ_0\left(\frac{\lambda_n\gamma_1}{\sqrt{\bar{\alpha}_1}}\right)\right)\left(Y_0\left(\frac{\lambda_n}{\sqrt{\bar{\alpha}_1}}\right)+\frac{\bar{k}_1\bar{Z}_L}{\sqrt{\bar{\alpha}_1}}\lambda_n Y_1\left(\frac{\lambda_n}{\sqrt{\bar{\alpha}_1}}\right)\right)\right]-\left[J_0(\lambda_n(1-\chi_{LS}))Y_1(\lambda_n)\left(\frac{\bar{k}_1}{\sqrt{\bar{\alpha}_1}}\lambda_n J_1\left(\frac{\lambda_n\gamma_1}{\sqrt{\bar{\alpha}_1}}\right)-BiJ_0\left(\frac{\lambda_n\gamma_1}{\sqrt{\bar{\alpha}_1}}\right)\right)\left(Y_0\left(\frac{\lambda_n}{\sqrt{\bar{\alpha}_1}}\right)+\frac{\bar{k}_1\bar{Z}_L}{\sqrt{\bar{\alpha}_1}}\lambda_n Y_1\left(\frac{\lambda_n}{\sqrt{\bar{\alpha}_1}}\right)\right)\right]-\left[J_1(\lambda_n)Y_0(\lambda_n(1-\chi_{LS}))\left(J_0\left(\frac{\lambda_n}{\sqrt{\bar{\alpha}_1}}\right)+\frac{\bar{k}_1\bar{Z}_L}{\sqrt{\bar{\alpha}_1}}\lambda_n J_1\left(\frac{\lambda_n}{\sqrt{\bar{\alpha}_1}}\right)\right)\left(\frac{\bar{k}_1}{\sqrt{\bar{\alpha}_1}}\lambda_n Y_1\left(\frac{\lambda_n\gamma_1}{\sqrt{\bar{\alpha}_1}}\right)-BiY_0\left(\frac{\lambda_n\gamma_1}{\sqrt{\bar{\alpha}_1}}\right)\right)\right]+\left[J_0(\lambda_n(1-\chi_{LS}))Y_1(\lambda_n)\left(J_0\left(\frac{\lambda_n}{\sqrt{\bar{\alpha}_1}}\right)+\frac{\bar{k}_1\bar{Z}_L}{\sqrt{\bar{\alpha}_1}}\lambda_n J_1\left(\frac{\lambda_n}{\sqrt{\bar{\alpha}_1}}\right)\right)\left(\frac{\bar{k}_1}{\sqrt{\bar{\alpha}_1}}\lambda_n Y_1\left(\frac{\lambda_n\gamma_1}{\sqrt{\bar{\alpha}_1}}\right)-BiY_0\left(\frac{\lambda_n\gamma_1}{\sqrt{\bar{\alpha}_1}}\right)\right)\right]=0 \tag{B.4}$$

References

[1] V.J. Lunardini, Heat Transfer with Freezing and Thawing, Elsevier, 1991.
[2] V. Alexiades, A.D. Solomon. Mathematical Modeling of Melting and Freezing Processes, Routledge, 2018.
[3] L.I. Rubinshteĭn, The Stefan Problem 27, American Mathematical Soc, 1971.
[4] D.A. Tarzia, A Bibliography on Moving-Free Boundary Problems for the Heat-Diffusion Equation, Instituto Matematico, Ulisse Dini, The Stefan and Related Problems, Firenze, 1988.
[5] I. Dincer, M.A. Rosen, Thermal Energy Storage: Systems and Applications, John Wiley & Sons, 2021.
[6] A. Cohen, Encyclopedia of Thermal Packaging, Set 1: Thermal Packaging Techniques, World Scientific Press, 2012.
[7] R. Viskanta, Heat transfer during melting and solidification of metals, ASME. J. Heat Transfer. 110 (4b) (1988) 1205–1219.
[8] I. Glassman, R.A. Yetter, N.G. Glumac, Combustion, Academic press, 2014.
[9] J.D. Plummer, M. Deal, P.B. Griffin, Silicon VLSI Technology: Fundamentals, Practice and Modeling, Pearson Education, 2009.
[10] T. Higuchi, Mechanism of sustained-action medication. Theoretical analysis of rate of release of solid drugs dispersed in solid matrices, J. Pharm. Sci. 52 (12) (1963) 1145–1149.
[11] V.R. Voller, M. Cross, Estimating the solidification/melting times of cylindrically symmetric regions, Int. J. Heat Mass Transf. 24 (9) (1981) 1457–1462.
[12] J. Stefan, Über die Theorie der Eisbildung, insbesondere über die Eisbildung im Polarmeere, Ann. Phys. 278 (2) (1891) 269–286.
[13] D.A. Tarzia, M.F. Natale, Explicit solutions to the one-phase Stefan problem with temperature-dependent thermal conductivity and a convective term. International journal of engineering science, Int. J. Eng. Sci. 41 (15) (2003) 1685–1698.
[14] M. Parhizi, L. Zhou, A. Jain, Theoretical modeling of solid-liquid phase change in a phase change material protected by a multilayer Cartesian wall, Int. J. Heat Mass Transf. 197 (2022), 123330.
[15] A. Jain, M. Parhizi, Theoretical analysis of phase change heat transfer and energy storage in a spherical phase change material with encapsulation, Int. J. Heat Mass Transf. 185 (2022), 122348.
[16] M. Parhizi, A. Jain, Solution of the phase change Stefan problem with time-dependent heat flux using perturbation method, J. Heat Transf. 141 (2) (2019).
[17] T.R. Goodman, J.J. Shea, The melting of finite slabs, J. Appl. Mech. 27 (1) (1960) 16–24.
[18] D.W. Hahn, M.N. Özisik, Heat Conduction, John Wiley & Sons, 2012.
[19] C. An, F.C. Moreira, J. Su, Thermal analysis of the melting process in a nuclear fuel rod, Appl. Therm. Eng. 68 (1–2) (2014) 133–143.
[20] H. Wang, C. An, M. Duan, J. Su, Transient thermal analysis of multilayer pipeline with phase change material, Appl. Therm. Eng. 165 (2020), 114512.
[21] A. Kumar, S.K. Saha, Thermal and structural characterizations of packed bed thermal energy storage with cylindrical micro-encapsulated phase change materials, J. Energy Storage 48 (2022), 103948.
[22] V.V. Mikova, G.I. Kurbatova, N.N. Ermolaeva, Analytical and numerical solutions to Stefan problem in model of the glaciation dynamics of the multilayer cylinder in sea water, J. Phys. Conf. Ser. 929 (1) (2017), 012103.
[23] Y.P. Shih, S.Y. Tsay, Analytical solutions for freezing a saturated liquid inside or outside cylinders, Chem. Eng. Sci. 26 (6) (1971) 809–816.
[24] J. Caldwell, Y.Y. Kwan, On the perturbation method for the Stefan problem with time-dependent boundary conditions, Int. J. Heat Mass Transf. 46 (8) (2003) 1497–1501.
[25] S. Kalaiselvam, M. Veerappan, A.A. Aaron, S. Iniyan, Experimental and analytical investigation of solidification and melting characteristics of PCMs inside cylindrical encapsulation, Int. J. Therm. Sci. 47 (7) (2008) 858–874.
[26] L. Bilir, Z. Ilken, Total solidification time of a liquid phase change material enclosed in cylindrical/spherical containers, Appl. Therm. Eng. 25 (10) (2005) 1488–1502.
[27] L.C. Tao, Generalized numerical solutions of freezing a saturated liquid in cylinders and spheres, AICHE J. 13 (1) (1967) 165–169.
[28] B. Izgi, M. Arslan, Numerical analysis of solidification of PCM in a closed vertical cylinder for thermal energy storage applications, Heat Mass Transf. 56 (2020) 2909–2922.
[29] A. Barba, M. Spiga, Discharge mode for encapsulated PCMs in storage tanks, Sol. Energy 74 (2003) 141–148.
[30] B.B. Mikic, W.M. Rohsenow, Thermal Contact Resistance, National Aeronautics and Space Administration, 1966. Report # DSR 74542-41.
[31] G. Krishnan, M. Parhizi, A. Jain, Eigenfunction-based solution for solid-liquid phase change heat transfer problems with time-dependent boundary conditions, Int. J. Heat Mass Transf. 189 (2022) 122693.
[32] M.A. Al-Gwaiz, Sturm-Liouville Theory and its Applications, 1st ed., Springer, London, 2008.
[33] M.D. Mikhailov, M.N. Özisik, Unified Analysis and Solutions of Heat and Mass Diffusion, Dover Publications, 1984.
[34] G.H. Golub, H.A. Van der Vorst, Eigenvalue computation in the 20th century, J. Comput. Appl. Math. 123 (1–2) (2000) 35–65.
[35] D. Anthony, D. Sarkar, A. Jain, Non-invasive, transient determination of the core temperature of a heat-generating solid body, Sci. Rep. 6 (1) (2016) 1–10.
[36] R.A. Seban, A.L. London, Experimental confirmation of predicted water-freezing rates, Trans. Am. Soc. Mech. Eng. 67 (1) (1945) 39–44.
[37] R. Siegel, J.M. Savino, Transient solidification of a flowing liquid on a cold plate including heat capacities of frozen layer and plate, National Aeronautics and Space Administration, 1968.